Evaluation of Refined Tribological Properties of Diamond Coated Cutting Tools Used in Machining of High-Strength Aluminum Alloys

Master thesis report regarding refined frictional & wear behavior of uncoated & CVD diamond coated WC-Co cemented carbide cutting tools used for machining of Al 7xxx alloys.

Masteruppsats om renodlade friktions & förslitningsbeteende hos obelagda & CVD diamant belagda WC-Co hårdmetallskärverktyg för bearbetning av Al 7xxx legeringar.

Christian Hultman

Karlstad University
Faculty of Health, Science & Technology
Department of Engineering & Physics
MSAE01, Master Thesis Project Work in Mechanical Engineering
Examiner: Mikael Grehk
Supervisor: Mikael Fallqvist
Date: 2022-07-02

Abstract

High strength aluminum alloys have for a long time been a popular material utilized in the automotive and aerospace sector due to coveted mechanical properties in terms of weight, strength, fatigue, and corrosion. However, tribological mechanisms such as tribo-film formation and material transfer during the metal cutting manufacturing process of aluminum impose significant reduction of machining and tool-life performance. Additionally, environmental aspects associated with metal cutting manufacturing has got more interest and pushed cutting tool development in new directions to meet increased customer demands. One possible way of achieving this, is the implementation and utilization of diamond based cutting tools which has been shown to perform well in machining of high strength aluminum. However, in depth knowledge regarding the tribological properties of diamond based cutting tools is currently lacking. Thus, the aim of this master thesis has been to investigate the refined tribological characteristics and properties of WC-Co cemented carbide cutting tools coated with synthetically grown CVD diamond. Tribological testing methods, such as frictional scratch/sliding, pin-turning, contact-zone temperature measuring, and longitudinal turning have been conducted to acquire extensive amount of research material in the form of test samples and data information. Furthermore, pin-turning tests were performed using a newly developed Tribojan pin-turning equipment and the performance of this was evaluated as a subgoal task. Specimen sample analysis have primarily been performed through LOM and SEM/EDS microscopy techniques. The results acquired from testing, microscopy analysis and data set evaluation have showed promising results in terms of frictional characteristic and material transfer properties regarding CVD diamond coated surfaces. The average CoF of CVD diamond sliding against an Alumec 89 aluminum alloy surface were somewhat lower as compared with similar sliding of a conventional uncoated WC-Co cemented carbide material. Furthermore, the frictional behavior and characteristic of CVD diamond appears to be more consistent and regular over longer sliding distances. The contact interaction between the CVD diamond coated surface and Alumec 89 appears to have a more abrasive nature due to the rough surface structure and material properties of the coating. The corresponding tribo-pair contact interaction with WC-Co cemented carbide shows more adhesive tendencies. Additionally, the contact-zone temperature development during pin-turning is shown to be somewhat lower during CVD diamond/Alumec 89 surface interactions. Regarding material transfer properties, CVD diamond are shown to perform well when interacting with high-strength aluminum. The amount of material adherence is significantly reduced on CVD diamond coated surfaces. During longitudinal turning using CVD diamond coated cutting tools, no significant wear was observed. On the other hand, evidence of both adhesive and abrasive wear was observed during turning using conventional uncoated WC-Co cemented carbide tools. Finally, tribological mechanisms acting during Tribojan pin-turning tests was shown to be relatively comparable with an actual machining operation, which indicate that the testing method perform well as compliment to standard frictional sliding and machining testing.

Sammanfattning

Höghållfasta aluminiumlegeringar har länge varit ett populärt material inom bil- och flygindustrin på grund av deras eftertraktade mekaniska egenskaper när det gäller vikt, styrka, utmattning och korrosion. Däremot medför tribologiska fenomen, så som tribofilmbildning och materialöverföring under metallskärande tillverkningsprocesser för aluminium, en betydande minskning av prestanda hos utrustning och skärverktygens livslängd. Dessutom har miljöaspekterna i samband med metallskärande tillverkning fått ökat intresse och därmed drivit utvecklingen av skärverktyg i nya riktningar för att uppfylla kundernas ökade krav. Ett möjligt sätt att uppnå detta är att införa och använda diamantbelagda skärverktyg, vilka har visat sig fungera bra vid bearbetning av höghållfast aluminium. Dock saknas det för närvarande djupgående kunskaper om de tribologiska egenskaperna hos dessa diamantbaserade skärverktyg. Syftet med detta examensarbete har därför varit att undersöka de förfinade tribologiska egenskaperna hos WC-Co skärverktyg av hårdmetall belagda med syntetiskt odlad CVD-diamant. Tribologiska testmetoder, så som friktionsskrapning/glidning, pinnsvarvning, temperaturmätning i kontaktzonen samt longitudinell svarvning, har genomförts för att samla in analysmaterial i form av prover och datainformation. Dessutom utfördes pinnsvarvningstesterna med hjälp av en nyutvecklad så kallad Tribojan-utrustning, vars prestanda har utvärderats som ett delmål i projektet. Analyser av provexemplar har huvudsakligen utförts med hjälp av mikroskopitekniker så som LOM och SEM/EDS. Resultaten från provning, mikroskopianalys och utvärdering av data har visat lovande resultat när det gäller friktions och materialöverföringsegenskaper för CVD-diamantbelagda ytor. Den genomsnittliga CoF för CVD-diamant som glider mot en yta av aluminiumlegeringen Alumec 89 var något lägre jämfört med motsvarande glidning av konventionellt WC-Co hårdmetallmaterial. Dessutom verkar friktionsbeteendet hos CVD-diamant vara mer konsekvent och regelbunden över längre glidsträckor. Kontaktinteraktionen mellan ytor av CVD-diamant och Alumec 89 verkar också ha en mer abrasiv karaktär på grund av diamantbeläggningens grova ytstruktur och materialegenskaper. Motsvarande kontaktinteraktion mellan Alumec 89 och obelagd WC-Co hårdmetall visar däremot mer adhesiva tendenser. Dessutom tenderar temperaturutvecklingen i kontaktzonen under pinnsvarvning vara något lägre vid ytinteraktioner mellan CVD-diamant och Alumec 89. När det gäller materialöverföringsegenskaperna visar sig CVD-diamant fungera bra vid interaktion med höghållfast aluminium. Materialets vidhäftning minskar betydligt på diamantbelagda ytor. Vid kontinuerlig longitudinell svarvning med diamantbelagda skärverktyg observerades inget betydande slitage. Å andra sidan hittades tecken på både adhesivt och abrasivt slitage under svarvning med konventionella obelagda WC-Co hårdmetallverktyg. Slutligen visade det sig att de tribologiska mekanismerna som verkade under Tribojan-pinnsvarvning vara relativt jämförbara med faktisk bearbetning, vilket tyder på att testmetoden fungerar bra som komplement till friktions och svarvtester.

Table of Contents

Abstract

Sammanfattning

1 Introduction 6

2 Project description 7

3 Theory 8

3.1 Contact between surfaces 8

3.2 Friction 8

3.2.1 Sliding friction 9

3.2.2 Friction of ceramic materials 9

3.3 Wear 10

3.3.1 Adhesive wear 10

3.3.2 Abrasive wear 11

3.3.3 Tribo chemical wear 12

3.4 Tribofilm formation 12

3.5 Principles of orthogonal turning and tribology in metal cutting 13

3.6 Materials 15

3.6.1 Aluminum-Zinc alloys of the 7xxx series 15

3.6.2 Cemented carbide 15

3.6.3 Polycrystalline PCD Diamond 16

3.6.4 CVD Diamond 17

3.7 Experimental tribological test methods & equipment 19

3.7.1 Scratch test 19

3.7.2 Pin-turning test 19

3.7.3 Turning & milling test 20

3.8 Technologies and methods of sample analysis 21

3.8.1 Sample preparation 21

3.8.2 Light Optical Microscopy 21

3.8.3 Scanning Electron Microscopy 22

3.8.4 Energy Dispersive Spectroscopy 23

4 Experimental work 25

4.1 Preliminary milling test 25

4.2 Sliding/scratch test 25

4.3 Tribojan pin-turning test 26

4.4 Longitudinal turning test 29

5 Analysis work 30

6 Results 31
6.1 Preliminary milling 31
6.2 Frictional comparison 32
6.3 Tribojan pin-turning 36
6.4 Longitudinal turning 41
7 Discussion 45
7.1 Initial observations 45
7.2 Frictional aspects of CVD diamond 46
7.3 Characteristics and mechanisms of material transfer 46
7.4 Tribological implication in longitudinal turning 47
8 Conclusion 49
9 Further work 50
10 Acknowledgements 51
11 Bibliography 52
12 APPENDIX A 55
13 APPENDIX B 58

1 Introduction

Out of all types of metals found in the earth's crust, aluminum Al is the third most abundant one and the use of aluminum in engineering applications gained real interest around the year 1886 when the first aluminum alloy was produced. Annual production volumes have been growing ever since, from just above 45 000 tons to more than 25 million in present day. This growth in production is mainly due to the industry demand and application within the aerospace and automotive sectors where aluminum alloys is one of the most dominating materials of use. Its popularity is due to advantageous material properties, such as high strength-to-weight ratios, low elastic modulus, good corrosion resistance and high fatigue strength. Additionally, aluminum alloys also exhibit relatively high strength at elevated temperatures. Furthermore, their low weight is especially desirable since it reduces the environmental impact due to lowered energy consumption and today the 2xxx, 6xxx and 7xxx alloy grades are currently responsible for most of the industrial machining activities [1].

To manufacture the final aluminum products used in the automotive and aerospace industry, metal cutting procedures such as turning, milling, and drilling are needed. Aluminum is considered as being relatively easy to machine. However, the increased strength of 7xxx grade aluminum leads to additional challenges during machining. Hence, manufacturing of high-strength aluminum products imposes higher demands on the cutting tools used during the metal-cutting procedures. Frequently used cutting tools today are made from cemented carbides consisting of a hard tungsten carbide WC phase, as well as a binder phase of primarily cobalt Co. The hard WC phase will provide the cutting tools with necessary strength and wear resistance, whilst the Co binder phase contributes with toughness and ductility. Hence, the overall mechanical properties of cutting tools in machining is greatly influenced by composition and WC particle size. Depending on the application, the grain size of WC can range between 0,3 µm to 40 µm and the Co content from 3 to 30wt%. However, a small grain size is usually preferable in most industrial metal cutting operations since this leads to increased hardness, which further result in improved wear resistance of the cutting tools. In addition, they also possess high heat resistance which generally makes WC-Co cemented carbide tools suitable for dry cutting and high-speed machining. However, cutting temperatures of around 600-1000 ºC can be attained during these machining conditions, which further give rise to thermally related friction and wear phenomena [2]. The friction and wear between the chip and tool tend to be higher at increasing cutting temperatures, which lead to higher wear rates that affect tool-life in a negative manner. WC-Co cutting tools also suffers from diffusion wear which leads to what is known as crater wear at the rake face of the cutting tool. This is a common wear mechanism associated with machining of aluminum alloys [3]. Additionally, the presence of build-up layers (BUL) at the tool rake faces are also common occurrences. This effect comes as a result from workpiece material being adhered to the tool surface which could lead to alteration of the tool geometry and furthermore cause harming levels of machine vibrations, as well as significant reduction of surface finish of the final product [1].

To improve quality and tribological characteristics of cutting tools used in conventional machining of aluminum alloys, deposition of synthetic diamond coatings onto the cutting tools have recently shown promising potential. In the modern era of material engineering, diamond is known as a unique coating material for complex-shaped and hard mechanical tools due to favorable tribological and mechanical properties like extreme hardness, high elastic modulus and good chemical stability. These properties all contribute to excellent wear resistance. Additionally, diamond based cutting tools have also shown some tendencies of possessing low coefficient of friction (CoF) values. However, any conclusive studies regarding these phenomena are currently lacking. Furthermore, the frictional and wear

behavior of engineering materials is quite complex and governed by numerous factors, such as the nature of the opposing surfaces as well as the surrounding environment. In this aspect, there is a need to study the underlying tribological behaviors and mechanisms governing frictional and wear characteristics of super-hard diamond coatings used in industrial machining operations [4].

2 Project description

The fundamental aim of this master thesis project is to investigate the tribological properties of WC-Co cemented carbide cutting tools which furthermore are coated with synthetic diamond through chemical vapor deposition (CVD), with the goal of gaining further knowledge about their applicability in dry machining of aluminum alloys. PCD diamond brazed cutting tools have already shown great potential in this regard. However, the knowledge and applicability of CVD diamond coated cutting tools in industrial machining are currently lacking. Hence, these types of cutting tools will therefore be of primary interest during this project. Experimental tribological testing methods such as frictional tests, pin-turning tests, as well as turning and milling tests will be conducted to acquire experimental information and data regarding the frictional and wear mechanisms involved during machining of aluminum alloys with CVD diamond coated cutting tools. Microscopy techniques such as light optic microscopy (LOM), scanning electron microscopy (SEM) and energy-dispersive X-ray spectroscopy (EDX) are primarily being utilized for data analysis. Furthermore, this project is conducted in close cooperation with SECO Tools AB located in Fagersta Sweden, which is a world leading company that specializes in machining solutions and metal cutting tool development for industrial machining operations.

3 Theory

The subject of tribology is a branch of science and technology that deals with interacting surfaces in relative motion. It includes the study of friction, wear, and lubrication, and is a key enabling technology in a wide range of engineering applications. Sliding or rolling between two surfaces that are in contact with each other can be found in almost any kind of real-world mechanical system, and the surface interactions taking place during these motions will often lead to decreasing performance of the mechanical system. Tribological mechanisms such as friction and wear will lead to loss of mechanical efficiency and progressive material removal that could have disastrous consequences in worst case scenarios. However, high material removal by wear is in some cases desirable. For example, in modern manufacturing processes such as grinding, turning, and milling, high wear is utilized in a controlled manner to shape commercial products and components into their final forms. Tribology is therefore one of the core disciplines within modern engineering and science since a deeper understanding of interacting surfaces is and continuously will be of great importance for the continued advancement and development of almost any type of applications within our modern society [5].

3.1 Contact between surfaces

Before delving into the concepts of friction and wear, it is worth discussing the microscopic aspects of surface-to-surface contacts. The surface of any kind of body in nature are never perfectly smooth. Some surface roughness (i.e., small scale irregularities at the surface), are always existing. As two plane and parallel surfaces are brought together, initial contact will first occur between the highest points located at the respective surface topography. These contact points are commonly known as *"asperities"* and are responsible for carrying the normal load acting on a surface during contact. Furthermore, they are also responsible for generating the frictional forces that may act between them. Thus, understanding the way that these asperities interact during varying loads is of fundamental importance in the theory of friction and wear since the concept is providing a physical explanation for many tribological observations [5].

3.2 Friction

During relative sliding between two surfaces in contact, the motion in a certain direction will be counteracted by a tangential force F_f known as the frictional force. For illustrational purposes, a simple model of this concept is illustrated in Figure 3.1.

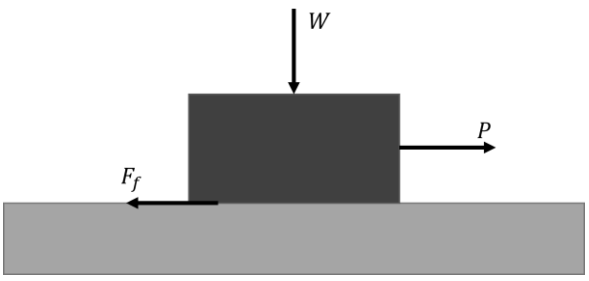

Figure 3.1: Forces acting during two-body sliding

The frictional force F_f is dependent on the normal load W and a coefficient μ, commonly denoted as the coefficient of friction (CoF). The CoF is defined as the ratio between the frictional force $F_{f,}$ and the normal load W given by the expression below:

$$\mu = \frac{F_f}{W}$$

Thus, the magnitude of the frictional force can be conveniently described by the CoF and can vary over a wide range of values depending on the type of materials involved during contact. Furthermore, environmentally factors such as air-humidity in the surrounding atmosphere could also have significant impact on frictional values. In lightly loaded bearings, for example, the CoF can be as low as 0.001 whilst it can reach values greater than 10 for two identically clean metal surfaces sliding in a vacuum. However, for most materials sliding in air, without any lubrication present, the CoF-value usually lies in the range of 0.1-1 [5].

3.2.1 Sliding friction

In the classical model of sliding friction, developed by Bowden and Tabor, the resultant frictional force between two surfaces in contact arises from two contributing force terms called the adhesion force F_a and the ploughing force F_p. The adhesion force F_a is developed at the real surface contact between two surfaces due to attractive forces acting at the asperity junctions. The influence of this force to the overall frictional force are mainly dependent on the environmental surrounding, cleanliness of the surfaces and the types of material in contact during sliding. Furthermore, the ploughing force F_p results from asperity deformation as harder asperities of one surface ploughs the softer ones of the other. Thus, both the adhesion force and the ploughing force could be described by two respective friction coefficients, namely the adhesion coefficient μ_a and the ploughing coefficient μ_p. The overall CoF could therefore be considered as the sum of μ_a and μ_p, as illustrated below [5].

$$\mu = \mu_a + \mu_p$$

It should be noted that the classical model of sliding friction is based on assumptions and simplifications which lead to discrepancies when comparing theoretical estimates to experimental measurements of the CoF. Work-hardening at the asperity junctions and so-called junction growth are two significant effects that will typically cause increased values of μ compared to theoretical calculations [5].

3.2.2 Friction of ceramic materials

Ceramic materials, or rather engineering ceramics, have come to be of great importance within modern manufacturing applications such as milling, turning, grinding, and drilling. The beneficial aspects of these materials are owed by their exceptional mechanical properties such as high strength, hardness, and stiffness. For the majority of cutting processes used in the manufacturing industry, engineering ceramics are commonly used as thick or thin coatings on substrates of nitride or carbide-based materials [5].

The major difference of mechanical properties in engineering ceramics compared to metals, are related to the interatomic forces in play on a microstructural level. The atomic bonding in ceramics is often a mix of ionic and covalent type, which lead to crystal structures having only a small number of independent slip systems available for dislocation movement. This will result in limited plastic flow at room temperature, and correspondingly less ductility when compared to metals. Thus, the asperity contact in ceramics will more likely be elastic rather than plastic. Plastic strains during asperity contact in sliding will therefore be generally small, and although adhesive forces exist, CoF-values of ceramics will not be as high as those observed in clean metal-to-metal sliding.

In addition to microstructural properties of ceramic materials, environmental factors are also affecting their frictional behavior. Although ceramic materials are generally known to have good chemical inertness, their surfaces are often susceptible to tribochemical reactions which lead to surface film formation that modify their frictional behavior. Surface film reactions is especially prominent during a sliding contact in which local high flash temperatures at the asperity contacts, exposure of atomically clean surfaces caused by some wear process and direct mechanical stimulation of the reaction are common mechanisms that would accelerate surface film formation. Furthermore, the effects of surface films could be very well marked for some ceramic materials. For example, measurements of friction in clean or repeated diamond-to-diamond sliding in a vacuum environment reach values of about 1. In air, however, the friction value is significantly smaller and usually ranges between 0.05 to 0.15. This effect is due to very low adhesive forces between the surfaces on account of adsorbed contaminations, together with small contributions of other dissipative processes.
Ceramic materials are also known to be quite brittle. Due to this property, widespread brittle fracture could occur in the contact-zone which would increase the friction, since it provides an additional mechanism for energy dissipation at the sliding contact [5].

3.3 Wear

As described in previous sections, friction is the resistance of motion encountered as two surfaces in contact are forced to slide in relative motion to each other. However, due to the motion and frictional properties of the respective materials in contact, progressive loss of material from one or both opposing surfaces will occur. This process is, within the tribological field of science, known as wear and is of substantial importance when considering the efficiency and operating lifetime of a product or component. The phenomenon of wear is quite a large subject and includes many kinds of mechanisms and processes. However, three main types are generally recognized – adhesive, abrasive and erosive wear. For this study, adhesive and abrasive wear will be the main topics of interest since these are commonly occurring during machining operations such as milling and turning. A brief description of these respective wear types is therefore given in the following sections [6].

3.3.1 Adhesive wear

Adhesive wear, or sliding wear, is concerned with degradation and removal of material that occurs when two solid bodies slide over each other. As the name suggest, adhesion plays an important role during this type of wear since it originates at the shearing contact between asperities of two solid counter surfaces. A simplified illustration of the adhesive wear mechanism is illustrated in Figure 3.2 where plastic flow at an asperity tip is followed by wear particle detachment.

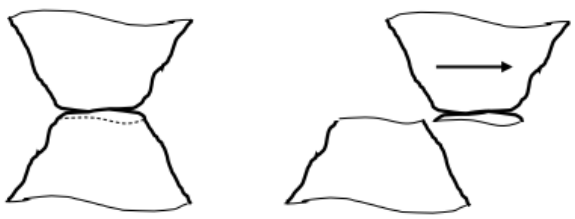

Figure 3.2: Illustration of the adhesive wear mechanism [6].

Elastic and/or plastic deformation of the asperities due to the sliding action will result in a contact area where atomic binding forces give rise to strong adherence in which surfaces essentially get welded

together. The tangential relative motion, brought upon by the sliding action, and adhesive forces will cause build-up of shear stresses which eventually lead to plastic shearing of successive layers in conjunction with shear crack propagation. Material removal is therefore caused by separation in the bulk of the asperities of the softer material that is present in the sliding contact. Hence, the controlling parameters of adhesive wear for a given material pair is the load, sliding distance, hardness of the softest material present in the contact and the probability of wear particle detachment when a contact weld is broken. It should also be mentioned that plasticity dominated adhesive wear is not yet fully understood. Several different mechanisms may very well be operating in sequence or simultaneously during the lifetime of a sliding system. Additional influences such as surface topology, composition and microstructure of the interacting materials, as well as the nature of possible surface-films or other adsorbed species, will all be significant factors during adhesive wear [2, 5].

3.3.2 Abrasive wear

The wear type known as abrasive wear are commonly characterized as displacement or removal of material from one surface, caused by hard particles or sometimes hard protuberances on a counterface, that are forced against and moves along the surface. The mechanisms of abrasive wear may involve both plastic flow and brittle fracture. Under some special conditions and circumstances, plastic flow may act alone, but often both occur simultaneously and together. Furthermore, abrasive wear will lead to significant plastic deformation of the surface material and often occur when one of the surfaces in contact are significantly harder than the other, or if hard particles are introduced in the surface contact interface. A distinction between two- and three body abrasion is thereby commonly made. These two abrasion types are illustrated in Figure 3.3 in which two-body abrasion is caused by hard protuberances on the counterface or hard particles attached to it. Three-body abrasion, on the other hand, is caused by loose hard particles present in the contact interface that are free to slide and roll in between two surfaces [2, 5].

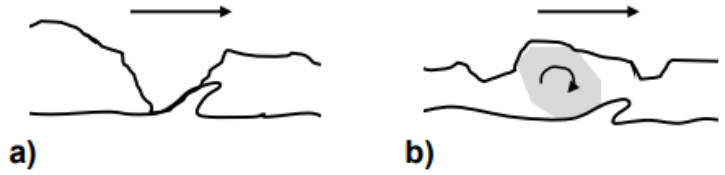

Figure 3.3: Description of abrasive wear types: a) two-body abrasion and b) three-body abrasion [2].

Abrasive wear can be further classified into different wear mechanisms such as micro cutting, micro fatigue, and micro chipping. However, hard sharp particles and asperities plays a key role in all these mechanisms. During sliding motion of two countersurfaces, the particles are pressed down into the softer material and causes plastic material flow. Due to the tangential movement, they will then plough through the surface of the softer material which further results in remaining scratches and grooves at the surface. The severity and rate of wear due to the abrasive ploughing action is dependent on the size, shape and hardness of the particles. Hard and sharp particles will have an increased ability to dig down into the softer material and thereby increase the amount of material removal during the ploughing action. Additionally, if the size of the particles is large, the rate of wear will be further increased. Note that the mechanisms associated with ploughing alone is not a wear mechanism, since no removal of material is taking place. It is just rearrangement of material [5]. Hence, the ploughing action will result in different wear mechanisms.

Material removal by abrasive wear can also occur due to brittle fracture in which the associated mechanisms differ from those involved during plastic flow. This phenomenon is often seen in brittle

materials where material removal is caused by lateral cracking, as illustrated in Figure 3.4. As sharp particles slide over a surface, plastic grooves will be formed, and lateral cracks will grow upwards from the sub-surface deformed region towards the free surface. This process is driven by residual stresses and material is removed as chips from the region bounded by the lateral cracks and the free surface [2, 5].

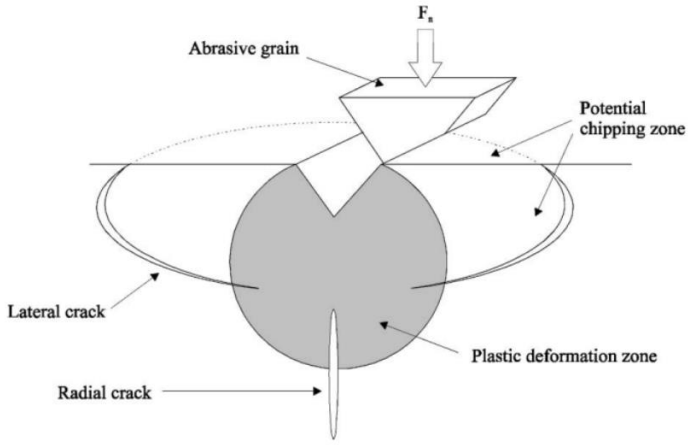

Figure 3.4: Schematic of brittle fracture formation during abrasive wear of brittle materials [7].

3.3.3 Tribo chemical wear

When discussing different wear mechanisms, chemical reactions tend to occur at the surfaces in contact that can both accelerate or deaccelerate the overall wear process. Material consumption due to chemical reactions in a contact interface are commonly referred to as tribo chemical wear. The governing factors for these processes are mainly environmental conditions in combination with mechanical contact mechanisms. Thereby, it is important to point out that the chemical action, such as diffusion or solution, should not be considered as a separate wear mechanism alone. Instead, the process always occurs in conjunction with other wear mechanisms. Thus, it is more correct to discuss the mechanical wear mechanisms firstly and consider the chemical effects, which will influence the material properties of the surfaces in contact, as a separate parameter [2].

3.4 Tribofilm formation

In relevance to the mechanisms present during friction and wear, tribofilm formation is an additional factor worthy of consideration. The environment between two surfaces in a sliding contact are quite extreme were local pressures, stresses and temperatures are high enough to break atomic bonds of even the strongest materials. Under such tribological conditions, the materials in contact will deform plastically and fracture on a micro scale. The outermost layers of two surfaces in contact will get mixed together due to transfer of atoms, molecules, or larger particles. This will further induce chemical reactions between the elements involved, which finally results in the formation of films or layers at the surface level of the materials in contact. Thus, the original surface material will be modified in which the tribological properties will change dramatically. Surface modifications such as topography changes, formation of micro-cracks, phase transformations, deformation hardening, and formation of oxides will in most cases alter the friction and wear properties of the original bulk materials [8].

Tribofilm formation is a complex phenomenon due to the many variables involved during a tribo-pair contact. It is multifaceted in its nature and is known through many names such as transfer films, built-up layers, third bodies, tribolayers, etc. However, tribofilms are usually divided into two subgroups known as *Transformation Type Tribofilms* and *Deposition Type Tribofilms*. In the first type, material transformation at the outermost region of a surface occurs due to diffusion, plastic deformation or frictional heating. Any sharp interface towards the underlying material is generally not present in these types of tribofilms. For the second type, tribofilms are usually formed on top of an existing surface by either pick-up of particles, adsorption of molecules or chemical reactions. In contrast to transformation type tribofilms, the processes occurring in deposition type tribofilms usually lead to a relatively well-defined interface between the film and underlying surface. Hence, effects such as adhesion and delamination become more enhanced for this type. The thickness of the tribofilms and layers included in each of the two subgroups, usually falls in the ranges between atomic monolayers up tens of micrometers [8].

3.5 Principles of orthogonal turning and tribology in metal cutting

Much of the theory related to pure tribology can be directly transferable to the process of metal cutting. However, the contact conditions and mechanisms acting in microscale is much more extreme during a metal cutting operation, which directly impose higher demands on the materials used. The process of metal cutting (or machining) is one of the most widely used manufacturing techniques utilized in the modern era of manufacturing. Using high-strength cutting tools made from materials such as tool-steels, high-speed steels (HSS) or cemented carbide hard-metals, high material removal is utilized to alter and form a workpiece of softer material into a desired shape and form. This is commonly performed by chip-cutting procedures such as drilling, turning, and milling. While much of the general theory behind metal cutting is applicable to each the three machining techniques mentioned, this section will be mainly focused on the physical aspects and mechanics of orthogonal turning [9, 10].

In orthogonal metal cutting, a turning machine of either conventional or CNC type is used to provide circular motion of a workpiece material. A cutting tool is then fed axially along the workpiece surface, in which material is continuously removed. The process is visualized by Figure 3.5. The volume of removed material per time unit are determined by the cutting speed v_c, feed f and depth of cut a_p. By this process, the final form of the workpiece material will thus have a circular geometry of rotational symmetry [9].

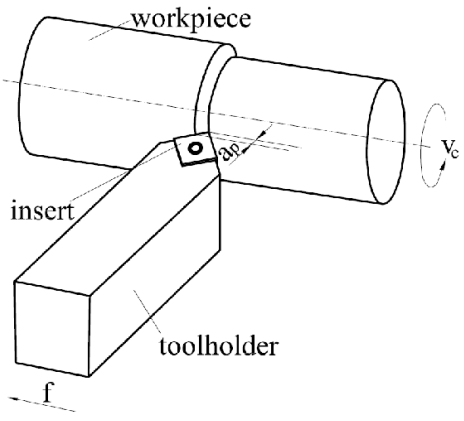

Figure 3.5: Schematic of a 2-D orthogonal turning operation [11].

As the cutting tool insert is fed along the workpiece surface, material is successively being removed by a process of shear where material flows against the so-called rake face of the tool insert until it finally leaves in the form of a chip. The material is deformed through plastic shearing along a shear plane lying at an angle θ with respect to the machined surface, as illustrated in Figure 3.6a. The angle θ can vary over a wide range depending on the present conditions during the cutting procedure. The geometry of the formed chip is defined by the depth of cut a_p and the rake angle α. Furthermore, the curvature of the chip is primarily dependent of the thickness of the chip, which additionally is determined by the feed rate. Thus, the cutting tool insert is of particular importance during a turning operation since it is responsible of both removing material as well as providing adequate surface finish of the machined component [10].

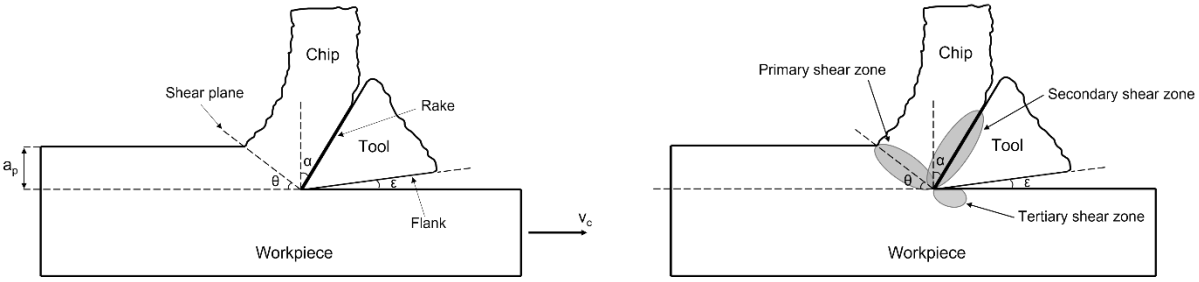

Figure 3.6: Schematic of the chip formation process. (a) Essential elements involved during orthogonal turning. (b) Illustration of shear zones.

During the chip formation process, significant amounts of mechanical work is being performed due to the high cutting forces developed around the vicinity of the cutting tool edge. The total amount of mechanical work performed during the workpiece/tool interaction is spread out over three zones as illustrated by Figure 3.6b. About one half to three quarters of the total mechanical work is dissipated as heat through plastic work in the primary shear zone. Most of this heat (~85%) is carried away by the chip and the rest is conducted in the workpiece. The remainder of the mechanical work is due to the friction at the interface between the rake face and the chip. The cutting condition in this area is significantly severe, where the surface of the freshly cut chip is initially free from any type of oxide film and the forces exerted by the tool is sufficiently high to cause plastic flow of material in the primary shear zone. Depending on the material and geometry of the cutting tool, as well as workpiece material and cutting conditions, adhesion between the workpiece material and the lower part of the cutting tool rake face may occur. In this situation the chip material will shear close to the tool surface. On the other hand, sliding along the whole rake face length may also occur in which additional plastic work is performed in the so-called secondary shear zone. Some of the heat generated in this zone is dissipated into the chip material but the majority will be conducted into the cutting tool [5]. Plastic material flow may also occur in a small region just beneath the tool tip between the flank face and workpiece surface. This region is termed the tertiary shear zone and develops as a result from adhesion or seizure [12].

The overall temperature distribution in the tool during a turning operation depends on the cutting conditions and the thermal properties of the tool and workpiece material respectively. Hence, temperature developments in the cutting tool insert will hugely influence the wear rate and several mechanisms of tool wear can show different dependencies with the temperature during metal cutting. For example, abrasive wear caused by hard particles present in the workpiece material is a purely mechanical process and material loss caused by this mechanism is relatively independent of temperature. However, the strength of the tool is weakened at high temperatures and the ability to sustain the cutting forces at the cutting edge would thereby be impacted. This phenomenon is known

as thermal weakening and could in worst case result in plastic deformation of the tool material. Additionally, chemical reactions at the tool surface, such as oxidation, is another example of thermally activated wear processes and could lead to rapid removal of the reaction product, resulting in what is known as built-up layer (BUL) formation. Furthermore, the combination of high contact pressure and lack of oxide at the freshly cut surface of the tool tip favors strong adhesion, which consequently could lead to cold welding of workpiece material on to the rake face of the tool. This mechanism is known as built-up edge (BUE) and is recognized as continuous accumulation of workpiece material along the cutting edge of the tool insert. This mechanism is especially common when machining ductile materials. However, the adhesion could, in some cases, be so strong that material detachment occurs within the tool rather than within the chip and subsequently result in adhesive wear [5].

3.6 Materials

Every tribological systems in the natural world involves a contact pair of materials. The materials could either be of the same or completely different types. Apart from mechanical and environmental factors, the tribological behavior is hugely influenced by the material properties of the two interacting surfaces in a tribo-pair contact. Hardness, mechanical strength, ductility, chemical affinity, thermal conductivity, etc. will influence the frictional and wear behavior of two materials in contact. These properties are furthermore dependent of the microscopical characteristics of the individual materials. Thus, material science is an essential part of tribology since it provides a way of further improving the quality and environmental impact of many applications such as more fuel-efficient engines in the automotive and aerospace sector, as well as increased performance of metal cutting processes within the manufacturing industry.

The following sections and paragraphs deal with the material aspects of this study. Descriptions of each respective material and their characteristics will be given to provide a deeper understanding regarding the frictional and wear mechanisms in play as they interact with each other.

3.6.1 Aluminum-Zinc alloys of the 7xxx series

Aluminum is the third most abundant metal in the earth's crust. In its natural form it has a face-centered cubic (FCC) structure exhibiting high ductility at ambient room temperature. It also has properties such as low density and high strength, leading to high strength-to-weight ratios. Compared to steel, aluminum has quite low melting temperature of about 660 ºC. However, as temperature of the surrounding environment decreases, the strength of aluminum increases while steel on the other hand becomes more brittle. Due to these primary properties, aluminum-based alloys are one of the most preferable materials of use in the aerospace and automotive industry. Particularly grades within the 7xxx-series. This category of aluminum alloys is primarily alloyed with zinc Zn, magnesium Mg and copper Cu in different contents depending on the desired properties. Furthermore, the alloys are heat treatable and often solution hardened to achieve exceptional mechanical strengths of up to 710 MPa, which is among the highest strength of all existing aluminum alloys. Additionally, the 7xxx-grade aluminum alloys also exhibit great ductility and toughness, as well as high fatigue and corrosion resistance [13, 1].

3.6.2 Cemented carbide

Cemented carbides are one of the most widespread powder metallurgy products in the world due to their outstanding combination of hardness and toughness. Cemented carbides come in a broad variability of compositions and microstructures and is mostly employed in applications where high wear resistance is of utmost significance. In fact, cemented carbide alloys composed of tungsten

carbides WC and cobalt Co are currently the most dominating material employed in the making of cutting tools for machining procedures within the modern manufacturing industry. These alloys consist of a hard tungsten carbide WC phase embedded in a ductile metal binder matrix of cobalt Co. The interplay between carbide and binder phases will determine the final microstructure and properties, which in general terms are described by the WC grain size and Co content. The exceptional hardness of WC cemented carbides are particularly dependent of the grain size, in which smaller grains provide higher hardness values as illustrated in Figure 3.7 [2, 3, 14].

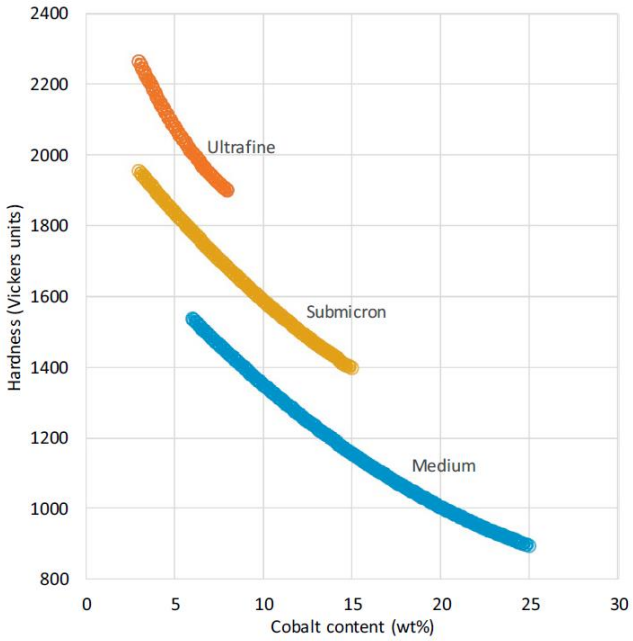

Figure 3.7: Hardness of cemented carbides with different grain sizes as a function of Co content [14].

Furthermore, the hard WC phase exhibit high melting point and a crystal structure which, regarding final cutting tool properties, will provide necessary strength and wear resistance whilst Co primarily brings toughness and ductility.
The carbide content in most of the commonly used cemented carbide structures is about 86 – 94 wt% and the remaining proportion consist of the Co binder phase. The grain size of WC ranges between 0.3 to 40 µm. However, for the metal cutting industry the grain sizes usually lie between 0.3 and 2 µm. [3, 2, 14].

During machining, uncoated WC-Co cemented carbide cutting tools are most preferable in dry-cutting conditions and high-speed machining due to their high hardness and resistance against heat and wear. However, during these machining conditions the cutting temperatures can reach values 600 - 1000 ºC, which consequently increases friction and wear rate of the tool [2]. This can cause what is known as crater wear at the chip flowing surface. Hence, thermally related friction and wear mechanisms can be provoked during metal cutting with WC-Co cemented carbide tools, which in some circumstances limits their use [3].

3.6.3 Polycrystalline PCD Diamond

In the development of modern cutting tools used in the manufacturing industry, polycrystalline PCD diamond brazed cemented carbide inserts have shown to be a popular and viable alternative over ordinary uncoated WC-Co cemented carbide tools. These cutting tools offer improved tribological properties like reduced friction and increased wear resistance which makes them particularly suited for machining of difficult-to-cut non-ferrous materials [15]. PCD is a synthetic diamond material manufactured through a high pressure and temperature (HPHT) sintering process. A fine diamond

powder consisting of either carefully controlled grain sizes, a wide distribution of grain sizes or multiple single sized grains are usually mixed with a binding material of cobalt. This mixture is then compacted into a so-called “green-body” that furthermore goes through the sintering process, where the Co acts as catalyst to accelerate formation of the PCD structure. It melts and infiltrates through the diamond grains to stimulate formation of diamond-to-diamond bonds. Hence, the final polycrystalline microstructure consists of two kinds of bonds – diamond-to-diamond and diamond-to-cobalt. A simplified illustration of the PCD synthesis is shown in Figure 3.8 [16, 17]. The sintering process results in a disc-shaped geometry of PCD bulk material, from which cutting tool edges can be cut from and finally brazed onto the cutting tool [17].

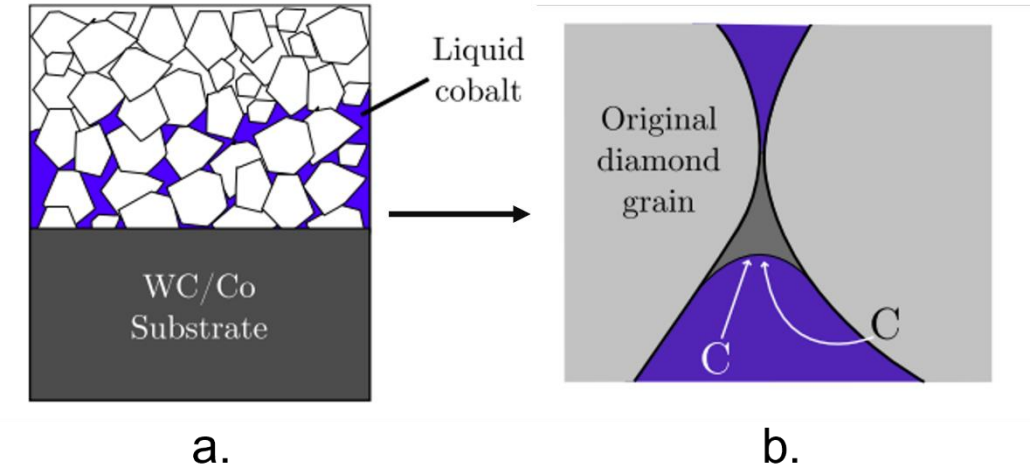

Figure 3.8: Illustration of diamond bonding by the PCD sintering process. a) liquid cobalt from WC-Co substrate filling voids between diamond grains. b) new diamond precipitates are sintered together [16].

This complex microstructure of original diamond grains, newly precipitated diamond, Co metal binder and various intermetallic phases leads to outstanding mechanical properties. PCD exhibits ultra-high hardness of up to 8000 HV, high thermal conductivity (560 W/mK), high elastic modulus and low CoF. These aspects are particularly desirable regarding machining and metal cutting, were the high hardness leads to excellent resistance against abrasion. Additionally, the amount of accumulated heat at the tool/chip and tool/workpiece interface are reduced due to the high thermal conductivity [16, 17].

3.6.4 CVD Diamond

As mentioned, PCD brazed cemented carbide tools have, since their introduction in the 70’s, been the best and in many cases only viable alternative regarding diamond based cutting tools. However, PCD tools suffer from high manufacturing costs due to the complex HPHT sintering process and the following finishing procedures. Additionally, the tools are also usually single tipped and limited to relatively few cutting styles. Hence, complex geometries of the cutting tool are almost impossible to achieve. These limitations have paved the way for the development and manufacturing of CVD diamond cutting tools. These tools consist of a cemented carbide (e.g., WC-Co cemented carbide) substrate material coated with either a thick or thin polycrystalline diamond film. The most prominent advantage of CVD diamond coatings, compared with PCD brazed and other single point cutting tools, is related to the cutting-edge geometry. CVD diamond coatings can be applied onto many different cutting-edge styles. Additionally, they can also incorporate complex chip breaker geometries which eliminates some of the depth-of-cut limitations that comes with PCD brazed cutting tools [15].

Deposition of the diamond film onto the WC-Co cemented carbide substrate surface can be done by various CVD processes. However, the so-called hot-filament chemical vapor deposition (HFCVD) technique are considered as the simplest and most reproducible way of growing diamond at low pressure. This process involves a gas mixture of about 0.1-2% methane CH_4 in hydrogen H_2 which enters a reactor that is evacuated to approximately 10-100 Torr. The gas flows through a metal wire or mesh made of either tungsten W, tantalum Ta, molybdenum Mo or rhenium Re and is furthermore heated to temperatures between 2000-2400 ºC. In these conditions, about 2-10% of H_2 molecules will be dissociated into single atomic hydrogen H. This together with CH_4 will result in series of pyrolysis reactions that result in the formation of various radicals and stable gaseous species [18]. These will then diffuse and react with the hot substrate surface inside the CVD chamber. Once a suitable reaction site is found, crystallites will be nucleated, and diamond growth begins. The growth continues upwards from the substrate surface in all three dimensions, creating a film of polycrystalline columnar grain structure. Radicals, such as methyl CH_3, are of particular importance during this process since they are the main contributors in forming the necessary C-C bonds within the diamond crystal lattice. Furthermore, the surface of the WC-Co substrate needs to be free from Co to increase the interfacial adhesion of the coating/substrate system. Remaining Co at the substrate surface can promote transformation of diamond into graphitic carbon phases which reduces the interfacial adhesion strength. Chemical etching is therefore commonly employed as surface pre-treatment to remove Co from the surface and produce complex cavities that strengthens the adhesion [4].

CVD coatings have shown to exhibit extremely good tribological characteristics in some applications reflected by low CoF, high hardness, high elastic modulus and excellent wear resistance. Additionally, by reducing the grain size from a microcrystalline nature to nano-crystalline, frictional properties of the CVD coating can be further improved. For industrial applications, such as cutting tools used for milling and turning, the main factor of interest is the adhesion quality of the coating/substrate system. Compressive residual stresses within the coating/substrate interface are commonly developed during the cooling stage of the CVD process due to differences in thermal expansion coefficients of diamond and WC-Co cemented carbide. Thus, the adhesion needs to be sufficiently strong to minimize the risk of micro-crack formation and coating de-lamination during the machining operation [4].

3.7 Experimental tribological test methods & equipment

An important aspect of experimentally based tribological studies is to choose the correct method and testing equipment to appropriately model and simulate the tribological system of interest. Commonly during tribological experiments the goal is to gain an understanding about frictional and wear mechanisms in the interface between two surfaces that slide in relative motion with each other. To obtain quantitative data used to draw important conclusions from, different kinds of so-called tribometers or tribotesters are usually used to measure friction and wear under controlled situations. The goal of the specific experiment dictates the selection of the tribometer. Furthermore, it is important to include all major parameters that impact friction and wear in the design of the experiment. Examples of such parameters are normal force, velocity and acceleration characteristics, direction of motion relative to the surface, system stiffness, surface cleanliness and roughness, contact temperature, relative humidity, lubricant properties, presence of loose particles, etc [19].

Tribological problems are present in almost all kinds of engineering fields and a wide range of commercial tribometers and tribotesters are available on the market that can be used to mimic different kinds of situations encountered in real world applications. However, special tribometers are in some situations designed to provide certain testing conditions, specific specimen simulations or component dimensions [19]. In this study, there are mainly three types of testing methods employed – scratch test, pin-turning test and milling-turning test. Each of the three methods are further described in the following paragraphs of this section.

3.7.1 Scratch test

The scratch test is an easily applied method to measure and evaluate the adherence and scratch resistance of thin hard coatings and bulk materials. The basics of this method consist of moving a stylus with a well-defined tip over the surface of the specimen [19]. Most often a constant normal stylus load is applied to the sample surface while it is displaced at constant velocity. This causes elastic and plastic deformation at the scratching point until damage occurs in the surface region. An illustration of the scratch test method is shown in Figure 3.9 [20].

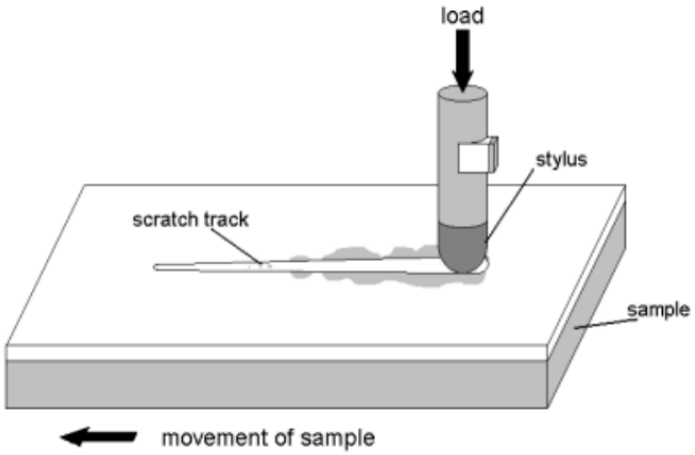

Figure 3.9: Simplified illustration of the scratch testing method [21]

3.7.2 Pin-turning test

So-called pin-on-disk or pin-on-ring methods are standard laboratory test set-ups used when studying sliding wear. Both these methods are characterized by repeated contact between two surfaces. However, although these test methods bring significant experimental advantages, the contact

conditions differ from those present at a tool-workpiece interface. For example, the standard pin-on-ring test suffers from poor performance due to insufficient toughness, strength, or wear resistance of the comparative tool material, which causes problems with data interpretation. Predictions of the wear resistance of cutting tool materials used in machining operations have thereby been unsuccessful using these conventional testing techniques. Modified versions, referred to as pin-turning tests, have instead been developed to better simulate and determine the wear mechanisms involved during true turning operations [22].

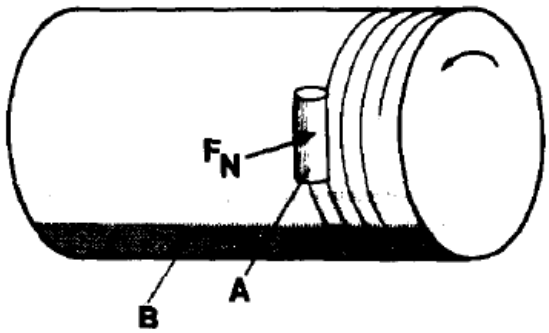

Figure 3.10: Illustration of the modified pin-on-ring set-up. Object A is allowed to continuously slide against fresh counter material introduced by surface B [22].

In the pin-turning configuration, the ring material shown as B in Figure 3.10 is considered as the workpiece material and is mounted as such in a standard lathe machine. The cylinder part A is mounted onto the tool holder and a spring loading system is furthermore used to control the normal force F_N. The frictional force F_f could furthermore be monitored by strain gauges under the duration of the test. In this specific example, the object pressed against the workpiece has a cylindric geometry. However, depending on the nature of testing, objects of different geometries can be used. Through this general set-up, wear testing could be conducted at the same spot of the workpiece (closed tribo-system), or by continuously introducing fresh counter material (open tribo-system) through the feed control feature of the lathe machine [22].

3.7.3 Turning & milling test

The contact between a workpiece material and the cutting tool is associated with severe and progressive wear due to material removal performed by the tool insert. Furthermore, the wear process in metal cutting is often quite complex and involve both mechanical, thermal and chemical interactions between the surfaces in contact. Hence, the characterization of wear and failure modes of cutting tools used for metal cutting in the modern manufacturing industry is of great importance [23].

The specific procedure of testing is largely influenced by which type of cutting process that is of interest. However, the general way is to basically perform the type of cutting process (turning or milling) in an appropriate machine while keeping one or several machining parameters (cutting speed, cutting depth, feed rate, etc) constant and then changing another relevant parameter. Observation of the effect caused by the specific machine parameter change can then be done through various kinds of measurement equipment and tribometers. For in depth observations, acquired test samples are also conveniently analyzed through some microscopy technique (e.g., LOM or SEM/EDX) to gain further understanding of the type of wear mechanism in play during the workpiece/tool tribo-pair contact [24].

3.8 Technologies and methods of sample analysis

This section summarizes the main theoretical aspects regarding equipment and methods used for sample analysis. The following paragraphs deals with topics such as sample preparation, Light Optic Microscopy (LOM), Scanning Electron Microscopy (SEM) and Energy Dispersive Spectroscopy (EDS) respectively. Note that the technologies and methods described are the primary ones utilized during the analysis work (section 5) of this project and does not cover the entire scope of analyzing methods currently existing in the modern day scientific and research field.

3.8.1 Sample preparation

To perform a good microstructural analysis with accurate and adequate results, the specimen needs to be properly prepared before entering any type of microscope. Sample preparation could be done through many types of techniques depending on the type of microstructural analysis preformed. However, mainly four steps are commonly utilized – sectioning, mounting, grinding and polishing, and etching. Sectioning is commonly performed through abrasive cutting in which the specimen is sectioned by a thin rotating disc. After sectioning, the sample often goes through the mounting step, which refers to embedding it in a mounting material (commonly a thermosetting polymer).
The third step of sample preparation is grinding and polishing, which is conducted to flatten and polish the surface to be examined. The specimen is commonly abraded in a graded sequence of abrasive grinding papers. Papers of increasingly finer particle size are used to grind and polish the surface to generate a scratch-free surface of mirror-like finish. Depending on the type of analysis conducted, chemical etching is sometimes further conducted to generate contrast between microstructural features in the specimen surface. Chemicals, referred to as etchants, are used to selectively dissolve certain areas of the specimen surface, with the main purpose of making the microstructure appear more distinct during analysis [25].

3.8.2 Light Optical Microscopy

The light optical microscope (LOM) is a type of microscope that, through a series of lenses, uses visible light to magnify images of small samples to be seen by an observer. The primary objective of a LOM is to examine microstructural features of a given material and is commonly referred to as metallography [25].

The basic principle of image formation in a LOM is exemplified in Figure 3.11, where a specimen is placed at position A, between one and two focal lengths f_1 away from an objective lens. The emitted light rays from the specimen object will converge at the first objective lens and subsequently being focused into a magnified inverted first image at position B. The light rays from this image will furthermore pass through a second objective lens, where they are further converged until finally being focused to form a viewable image at position C [25].

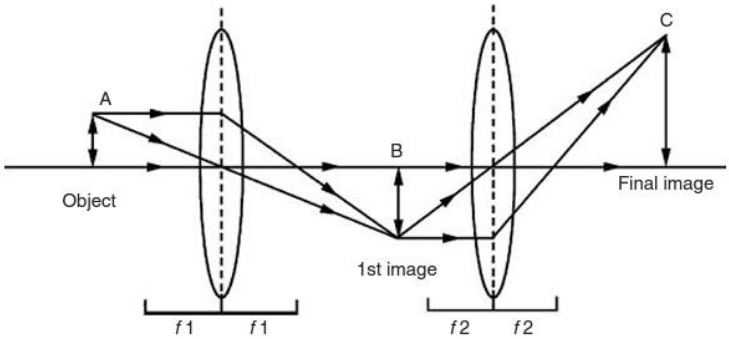

Figure 3.11: Principal illustration of image formation in light microscopy [25].

3.8.3 Scanning Electron Microscopy

In the area of modern-day research and science, the scanning electron microscope (SEM) is one of the most widely used types of electron microscopes due to its outstanding image processing capability and relative ease of use. It is primarily used to examine the microscopic surface structure of a given material, in which a focused electron beam scans over the surface area of a specimen sample. This creates a high-resolution SEM image with a three-dimensional appearance due to the exceptional depth of field obtained. The basic working parts of an SEM is illustrated by Figure 3.12 and consists of a long column in which an electron gun along with a series of electromagnetic lenses and apertures are placed. The electron gun generates an electron beam that is condensed as it passes through the first and second condenser lenses. The objective lens then focuses the condensed electron beam into a fine probe which finally are used to scan the surface of a specimen placed at the bottom of the column [25].

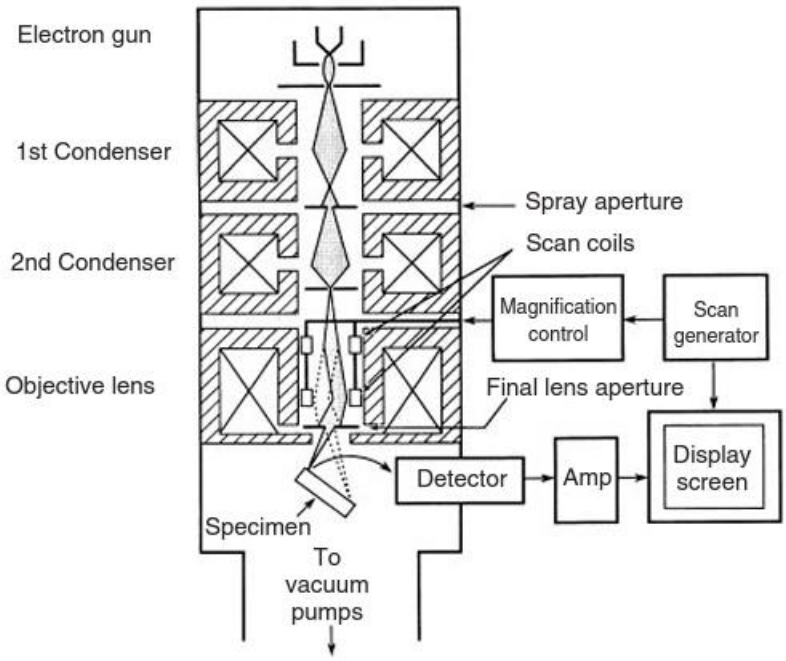

Figure 3.12: Basic setup of the SEM microscopy equipment [25].

As high-energy electrons from the electron beam strikes the surface of the specimen, electrons will be scattered by the atoms present in the specimen. Based on the trajectory of the scattered electrons they could either be of elastic or inelastic type. The elastic type of scattering is commonly denoted as backscattered electrons (BSE) which typically are deflected from the specimen at large angles with little kinetic energy loss. The inelastic type of scattering produces what is known as secondary electrons (SE), which are deflected at smaller angles with significantly lower levels of kinetic energy. Both SE: s and BSE: s is used as signal sources in the formation of an SEM image. However, they provide different results based on which feature that is of interest. SE: s are the primary signals for achieving topographical surface contrast while BSE: s provides compositional contrast. The reason for this is that SE: s and BSE: s collected by the detector originate from different regions in the specimen sample. This is illustrated by the schematic in Figure 3.13 which shows the interaction volume from which the electrons scatter as the high-energy electron probe hits the specimen surface. The size of the volume increases with the energy of the incident electrons in the probe. As previously mentioned, SE: s is the product of inelastic scattering having quite low energy level. Hence, they can only escape from a region between 5 – 50 nm beneath the specimen surface. In contrast, the energy levels of BSE: s are significantly higher since they are generated through elastic scattering. This enables them to escape from larger depths of the interaction volume, as shown in Figure 3.13. Additionally, the

spatial resolution of an SEM is dependent of the size of the entire interaction volume from which electrons can escape from. Hence, an image formed by SE: s should have better resolution than one formed from BSE: s [25].

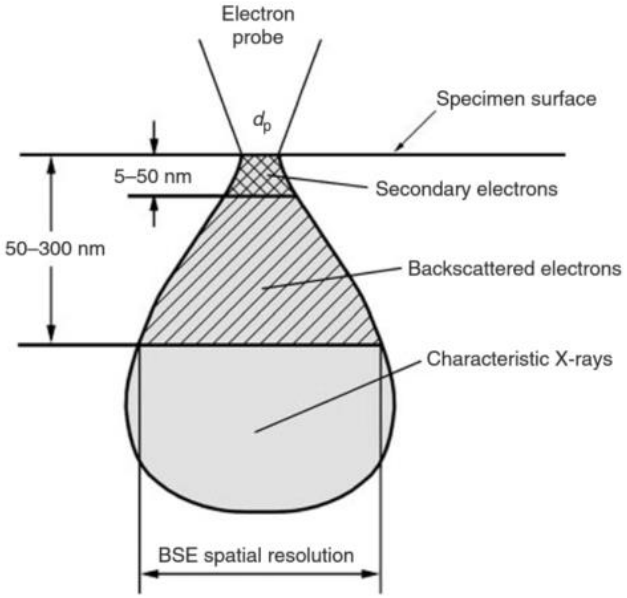

Figure 3.13: Schematic of electron interaction volume below a specimen surface [25].

3.8.4 Energy Dispersive Spectroscopy

A modern SEM microscope are often included with a so-called X-ray spectrometer of EDS type, used to perform elemental analysis while examining the microstructure of materials. The fundamental of this technique is based on the physical principles of characteristic X-ray generation. If an incident electron with sufficiently high kinetic energy can excite an electron located in the inner shell of an atom to a higher energy state, the vacancy left in the inner shell will immediately be filled by an electron from an outer shell. As the outer shell electron fills the vacancy, energy will be released in the form of emitted X-ray. The beam of X-ray will have a very specific wavelength or photon energy depending on which element it is emitted from. This process is further illustrated in Figure 3.14 and utilized when preforming elemental analysis of a specimen. The result of the analysis is commonly presented in an EDS spectrum which shows the intensity of characteristic X-ray lines across the X-ray range. However, it is important to realize that elements detected in an EDS spectrum represent those present at a distance down in the specimen and not directly at the surface. That is, the characteristic X-rays are excited from a volume under the surface rather from an area on the surface [25].

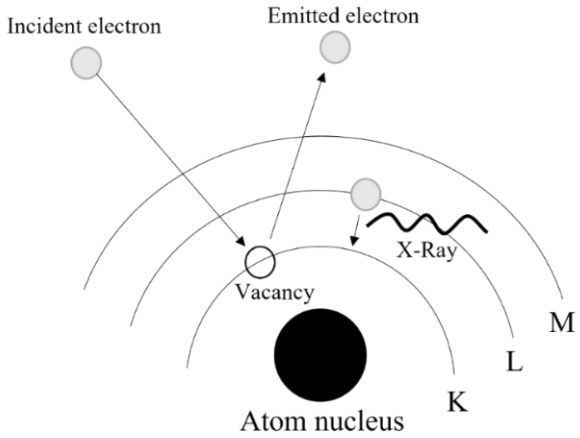

Figure 3.14: Physical principle of characteristic X-ray generation.

4 Experimental work

This section describes the series of methods and tests performed during the experimental phase of the project. Information and data gained from these tests provide the foundation and framework for further analysis of the refined tribological behavior and properties regarding CVD diamond coated cutting tools. Three types of tests were performed and is described in the following subsections of this paper.

4.1 Preliminary milling test

Since the knowledge regarding high-speed machining of aluminum using diamond based cutting tools are currently lacking, preliminary milling test was performed. Hence, the intention of this test was primarily to acquire knowledge basis regarding the milling operation, materials of interest and the overall tribological mechanisms in play. Milling operations were conducted using a Haas VF 2 three axis CNC milling machine with a maximum rotational speed of 8000 rpm. A milling cutter body of type A R220.69-0050-12-5AN with diameter 63 mm were used during all preformed milling tests. Cutting tools used during testing were of type uncoated and PCD brazed WC-Co cemented carbide. Note that the uncoated tools were indexable and the PCD brazed tools were non-indexable. Geometry description of the cutting inserts used are illustrated and summarized by Figure 12.1 and Table 12.1, APPENDIX A. Furthermore, all milling tests were performed using constant machine parameters given by Table 12.2, APPENDIX A. Two rectangular blocks of 6082 and Alumec 89 grade aluminum alloys, with dimensions 150x50x50 mm and elemental compositions given by Table 4.1, was chosen as workpiece materials.

Table 4.1: Elemental compositions for aluminium 6082 and Alumec 89 grade alloys.

Aluminum 6082 grade	**Si**	**Fe**	**Cu**	**Mn**	**Mg**	**Cr**	**Ni**	**Zn**	**Ti**	**Zr**	**Al**
Min	0,7	-	-	0,4	0,6	-	-	-	-	-	Bal
Max	1,3	0,5	0,1	1,0	1,2	0,25	-	0,2	0,1	-	Bal
Alumec 89	**Si**	**Fe**	**Cu**	**Mn**	**Mg**	**Cr**	**Ni**	**Zn**	**Ti**	**Zr**	**Al**
Min	-	-	1,5	-	2,1	-	-	5,7	-	0,10	Bal
Max	0,12	0,15	2,0	0,10	2,6	0,05	0,05	6,7	0,06	0,16	Bal

Shoulder milling of the workpiece blocks were conducted using each of the respective cutting tool inserts in four different combinations. For each combination of workpiece material and tool insert, the number of passings over the processed aluminum surface was altered between 1 and 10. The tool inserts used during each respective operational test run, along with the chips formed during the milling procedure, were collected and stored for further analysis. A detailed description regarding each combination of workpiece material and tool inserts, together with the number of workpiece surface passings during the operational test runs are provided by Table 12.3, APPENDIX A.

4.2 Sliding/scratch test

Scratch tests of uncoated and CVD diamond coated WC-CO cemented carbide tribo-pins sliding across an as-polished Alumec 89 aluminum surface were preformed using a commercial Anton Paar Revtest equipment©. An illustration of the test setup is shown by Figure 4.1, in which each respective tribo-pin type was initially mounted into a sample holder located above the polished aluminum surface. The tribo-pins were furthermore pressed and moved over the surface using a constant normal

load of 10 N and a relative sliding speed of 10 mm/min. A 10 mm sliding distance were set and each test were performed under dry sliding condition at room temperature. Three sliding tests on each respective tribo-pin type were performed. Note that new sliding tracks were created during each respective test. Hence, each individual sliding test were performed with fresh material of the counter surfaces. The CoF for each test were recorded using the Anton Paar Revtest© equipment accompanied computer software.

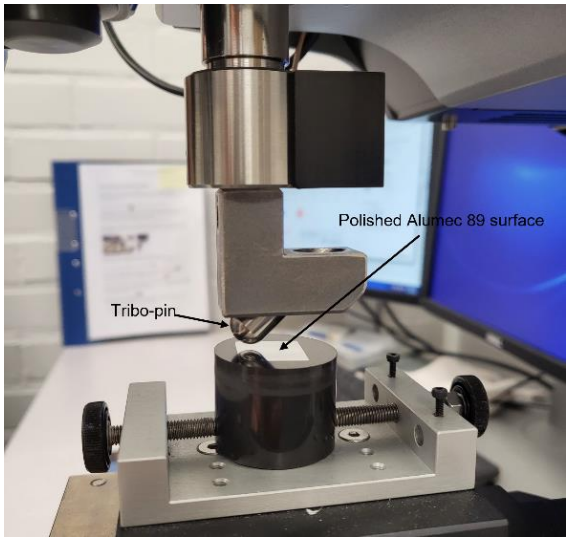

Figure 4.1: Scratch test sample setup.

4.3 Tribojan pin-turning test

Pin-turning tests were performed by the utilization of the so-called Tribojan equipment together with uncoated as well as CVD diamond coated WC-Co cemented carbide tribo-pins. Complete specifications regarding chemical composition, average WC-grain size and hardness values associated with the tribo-pins used are summarized in Table 4.2. Additionally, the diamond coating thickness is approximately 8 µm. An illustration of the Tribojan equipment and geometry of the tribo-pins is shown in Figure 4.2. Testing was performed on a solid cross-sectional circular bar of Ø160 mm, made of the aluminum alloy Alumec 89. Elemental composition of this material is given by Table 4.1.

Table 4.2: Technical specifications regarding diamond coated and uncoated WC-Co cemented carbide tribo-pins.

Type	**WC [wt%]**	**Co [wt%]**	**Cr [wt%]**	**V [wt%]**	**Vicker hardness [HV10]**	**Average grain size [µm]**
Diamond coated	93,5	6	0,4	0,1	1900	0,6
Uncoated	89,6	10	0,4	-	1600	0,8

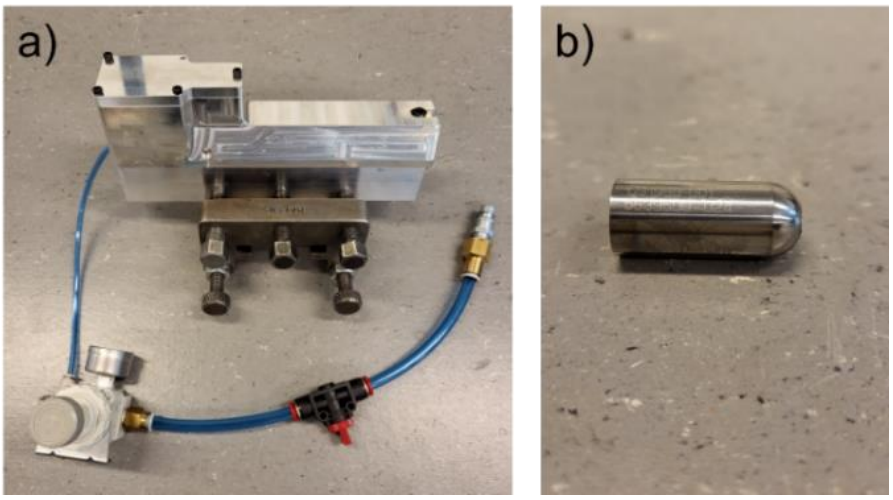

Figure 4.2: Illustration of the modified pin-turning test equipment were a) shows the Tribojan mechanism and b) shows the tribo-pins.

The Tribojan were fixed in a toolholder and mounted into a conventional Colchester Triumph 2500 turning machine with a maximum rotational speed of 2500 rpm. The tribo-pins were mounted and locked into a separate holder located at the end of the Tribojan mechanism. An illustration of the test setup is illustrated in Figure 4.3.

Figure 4.3: Illustration of the pin-turning test setup.

Two types of testing methods were preformed – closed and open pin-turning. In closed pin-turning, the workpiece material was set to rotate at a pre-defined rotational speed. The tribo-pins were then pressed against the workpiece material and held in the same axial position for a given time duration. Air-pressure was used to release the spring-loading mechanisms and push the tribo-pins against the surface of the workpiece material. The air-pressure were controlled by a pressure-valve and set to 1.3 MPa which corresponds to a pressing force of 10 N. The pressing force were held constant for the entire duration of contact between pin and workpiece. A total of 24 tests on eight separate tribo-pins (Four uncoated and four CVD diamond coated WC-Co cemented carbide tribo-pins) were preformed

using this method. The pins were tested at two different rotational speeds, generating two corresponding sliding speeds of 600 and 1200 m/min. For each sliding speed, the contact time of the pin/workpiece interaction was varied between 5 and 30 s. Three test runs per tribo-pin under each specific parameter setting were conducted to provide adequate statistical results. A description of the parameter settings for the uncoated and CVD diamond coated WC-Co cemented carbide pins are summarized by Tabell 4.3.

Tabell 4.3: Description of parameter settings and conditions regarding the Tribojan pin-turning method with static tribo-pin motion.

Test nr	Pin-material	Cutting speed [m/min]	Contact time [s]
1	Uncoated	600	5
2	Uncoated	600	30
3	Uncoated	1200	5
4	Uncoated	1200	30
5	Coated	600	5
6	Coated	600	30
7	Coated	1200	5
8	Coated	1200	30

The open pin-turning method was performed in a similar manner, with the addition of allowing axial movement along the workpiece surface. Note that only one test in this configuration was performed, since the purpose of the test was to only evaluate the performance of the Tribojan equipment. Testing was performed by utilizing the feed feature of the turning machine, in which an uncoated WC-Co cemented carbide pin were simultaneously pressed against and moved along the surface of the workpiece material. The turning machine was set to a corresponding cutting speed of v_c = 600 m/min and feed motion of f = 1.2 mm/rev. Feed motion was first initiated whereby the air-valve on the Tribojan were opened, allowing the tribo-pin to be pressed against the rotating workpiece at a constant normal load of F_N = 10 N, while simultaneously moving axially along its surface.

Temperature measurements near the contact-zone between tribo-pins and workpiece during closed pin-turning operations were also conducted. Using insulating tape and thermal paste, a thermocouple wire of type k with a sensitivity of 1200 ºC were taped on to the tips of one uncoated and one CVD diamond coated WC-Co cemented carbide tribo-pin respectively. The setup is exemplified by Figure 4.4. The pin/thermocouple setup were further mounted into the pin-holder mechanism of the Tribojan equipment (Figure 4.3) whereby closed pin-turning tests, as previously described, were conducted. The pressing normal force were set to F_N = 10 N and the rotational speed of the workpiece material was set to correspond with an equivalent cutting speed of v_c = 1200 m/min. Each temperature measurement was recorded over a 30 second period of sliding contact interaction between tribo-pins and workpiece material. Note that the placement of the thermocouple was approximately 3 mm from the pin/workpiece contact point during each test operation. The thermocouple was furthermore connected to a Pico Thermo Couple Data Logger sensor device used to measure and record the temperature development in the contact-zone during the pin/workpiece sliding interactions.

Figure 4.4: Illustration of tribo-pin/thermocouple setup. Tape is used to hold the thermocouple wire in the correct position. Thermal paste (white substance) is used to increase thermal conductivity and subsequently improve temperature reading signal.

4.4 Longitudinal turning test

Standard turning tests were utilized through continuous longitudinal cutting operations performed in a 2-axis Okuma SPACETURN LB4000 EX II CNC lathe machine. Specific performance data associated with the machine is given by Table 12.5, APPENDIX A. Turning operations were performed on a solid circular Alumec 89 aluminum bar with an initial cross section of Ø160 mm. Indexable cutting tool inserts of uncoated, CVD diamond coated and PCD brazed WC-Co cemented carbide were used. Geometry descriptions with accompanied values for each tool insert is summarized by Figure 12.2 and Table 12.6, APPENDIX A. Descriptions regarding the specific geometric units are explained by Table 12.7, APPENDIX A. Furthermore, all turning operations were preformed using an indexable toolholder of type SDJCL2525M11. A cutting depth of a_p = 0.5 mm and a feed rate of f = 0.1 mm/rev were set as constant cutting parameters during all turning operations performed. Continuous turning for t_c = 60 s with a cutting speed of v_c = 1200 m/min were conducted using each of the three cutting tool types respectively. The chips formed after turning with each type of tool inserts were collected and stored for further analysis. This procedure was furthermore repeated in which the cutting speed were changed between 900 and 600 m/min respectively. However, due to a limited number of cutting tools, only three cutting operations with a cutting speed of 1200 m/min and one with 600 m/min for 60 s were preformed using the PCD brazed tool type. The test procedure was repeated for the uncoated and CVD diamond coated WC-Co cemented carbide tools, whereby continuous turning instead were conducted for t_c = 5 s. All cutting operations in this longitudinal turning test were performed in a dry machining environment only. Further details are summarized by Table 12.8, APPENDIX A.

5 Analysis work

Test samples used in the experiments were analyzed through microscopy techniques such as LOM, SEM and EDS, as described in section 3.8. This to acquire clear and accurate illustrations regarding the observed tribological mechanisms. Primary test samples of tribo-pins and cutting tool inserts were prepared through a three-step cleaning process, in which they were placed in plastic cups filled with alcoholic based solutions and cleansed in an ultrasonic machine for approximately 15-20 min during each step. Acetone, isopropanol, and ethanol were used in each respective cleaning step. Large samples acquired from the Alumec 89 workpiece and used for surface analysis of the tribo-pin/workpiece interaction did go through an abrasive cutting step prior to the cleaning process. Furthermore, a special type of sample holder, illustrated in Figure 12.3, APPENDIX A were manufactured to achieve ease of sample mounting, as well as standardize the SEM analysis of the cutting tools.

Alumec 89 test specimens for frictional and metallographic analysis were prepared through abrasive cutting, in which small samples of rectangular shape were created using a Struers Setcom-50 cutting machine. The specimens were further mounted in an Struers Citopress-1 pressing machine, by which the specimens were embedded in 20 ml polymeric powder of type Polyfast and mounted under a pressure and temperature of 250 Bar and 180 ºC respectively for 5 minutes. Grinding and polishing of the samples were furthermore conducted using a Struers TegraPol-21 grinding equipment. Note that frictional scratch testing was performed prior to being cleansed through the three-step process described previously. The specimen was furthermore analyzed using in an JEOL JSM-7900F SEM microscope. The metallographic specimen went through an additional etching process after polishing, in which the sample were heated up to about 70 ºC by placing it on an Struers Drybox 2 heating stage. Etching for 40 s were done using a chemical solution of 25 ml nitric acid mixed in 75 ml distilled water. Metallographic analysis of the as-polished Alumec 89 surface were conducted using the JEOL JSM-7900F SEM equipment.

Data representation of results gathered from the frictional and thermal measurements were done using Microsoft Excel as computational software.

6 Results

This section summarizes the most relevant results gathered from the experiments and analysis work performed throughout the project. The results are presented in the form of microscopy pictures, graphs and charts, along with descriptive text explaining the identified tribological mechanisms. Note also that some data and information relevant to this section are placed in Appendix B, which will be referenced throughout the text when necessary. The results acquired from each respective experiment are presented in four subsections – Preliminary milling, Frictional comparison, Tribojan pin-turning, and Longitudinal turning.

6.1 Preliminary milling

Results regarding the preliminary milling test, as described in section 4.1, are presented in this paragraph. The focus of this analysis is to attain some initial information about the tribological behavior of uncoated and diamond coated WC-Co cemented carbide cutting tools used during a typical industrial machining process.

The main tribological mechanism observed in the surface analysis of the uncoated WC-Co cemented carbide cutting tool edges are BUL and BUE formation, as shown in Figure 6.1. BUL formation (i.e., regions of adhered aluminum on tool surfaces) is observed after machining both aluminum grade types. However, the characteristics of material transfer is more uniformly distributed along the cutting edge when machining 6082-grade aluminum, as illustrated by Figure 6.1a. Additionally, no significant BUE formation is observed in this case. Machining of Alumec 89 aluminum is seen to result in more randomly distributed regions of adhered aluminum on the cutting tool edge, as illustrated in Figure 6.1b. The regions of BUL: s also appears to be thicker in comparison with the tool used to machine 6082-grade aluminum. Furthermore, some BUE formation is found close to and along the cutting tool edge when machining Alumec 89, as opposed to 6082-grade aluminum.

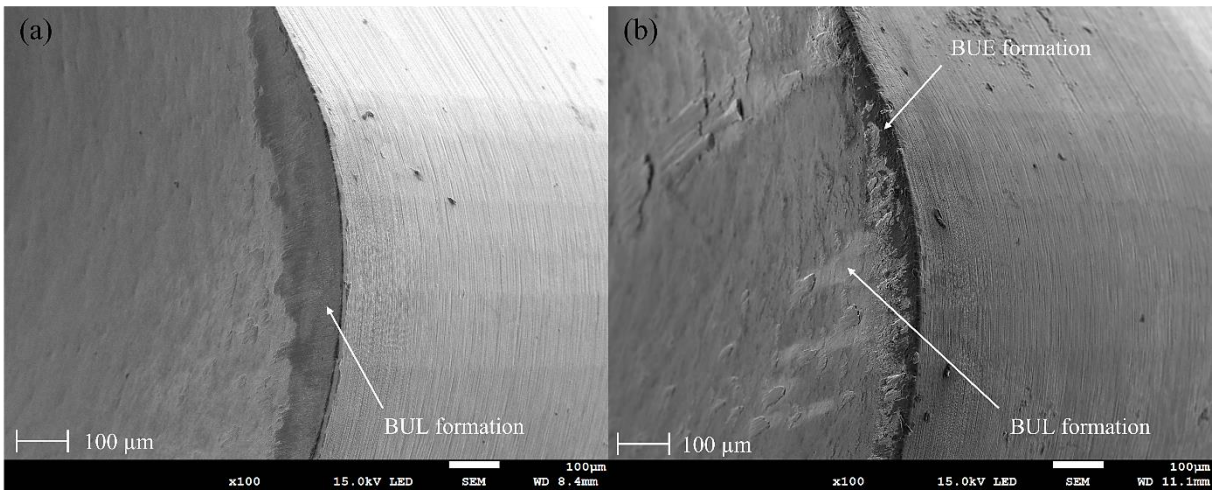

Figure 6.1: Cutting edge comparison of uniform WC-Co cemented carbide tools after machining two grade types of aluminum workpiece materials. (a) Machining of 6082-grade aluminum. (b) Machining of Alumec 89 grade aluminum.

Surface analysis of PCD brazed cutting tools used during milling operations conducted on both aluminum types are shown in Figure 6.2. Note that the cutting edge shown in Figure 6.2a is remained intact during milling of 6082-grade aluminum, whilst catastrophic failure has occurred at the tool tip when machining Alumec 89, as illustrated by Figure 6.2b.

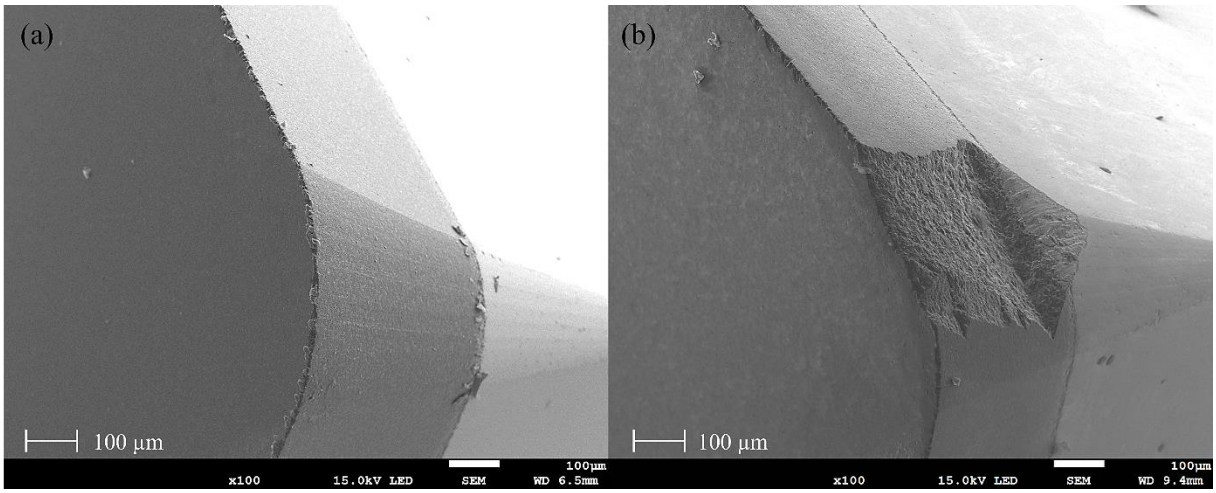

Figure 6.2: Cutting edge comparison of PCD diamond brazed cutting tools after machining two grade types of aluminum workpiece materials. (a) Machining of 6082-grade aluminum. (b) Machining of Alumec 89 grade aluminum.

The amount of material transfer, in terms of BUL formation along the cutting edge of the PCD brazed cutting tools, is found to be significantly less compared to the uncoated WC-Co cemented carbide tools. Additionally, the thickness of generated BUL: s is small, as evident by the SEM images shown in Figure 6.3. These images are taken using a lower acceleration voltage of the SEM equipment to increase surface sensitivity and subsequently make any adhered aluminum material appear more enhanced. Regions of both BUL and BUE are found on the rake face and along the cutting edge of the PCD brazed tool used to machine 6082-grade aluminum, as highlighted in Figure 6.3a. BUL formation is also observed when machining the Alumec 89 material, illustrated in Figure 6.3b. However, no apparent BUE is found in this case.

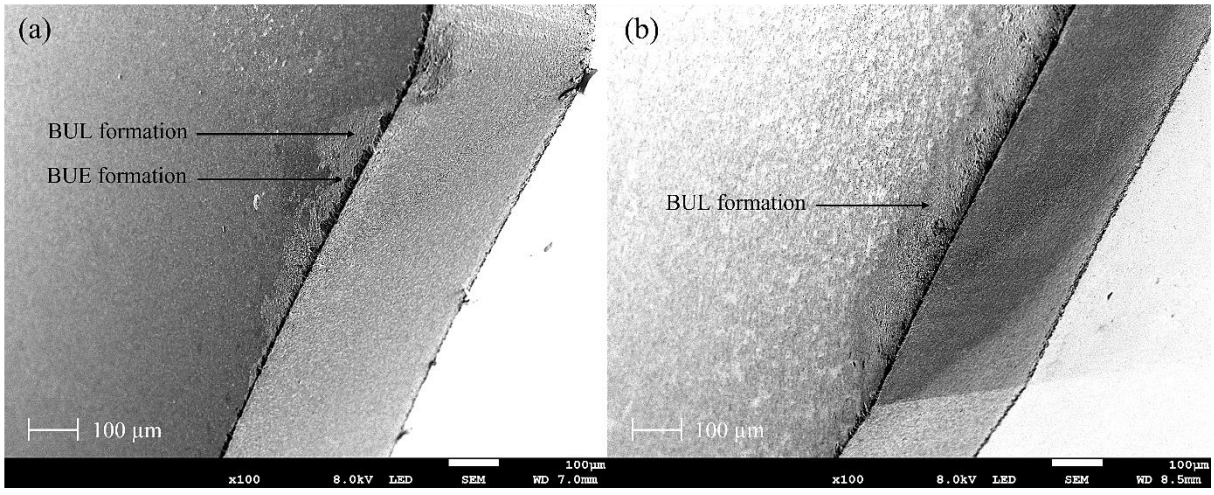

Figure 6.3: Examples of adhered aluminum onto PCD diamond cutting tools. (a) BUL and BUE formation after machining 6082-grade aluminum. BUL formation after machining Alumec 89.

6.2 Frictional comparison

A Comparison between the frictional behaviour of uncoated and CVD diamond coated WC-Co cemented carbide tribo-pins sliding against an as-polished aluminum surface of Alumec 89 grade, as described in section 4.2, are summarized in Figure 6.4 and Figure 6.5. A micrograph of the as-polished Alumec 89 test sample is shown by Figure 13.1, APPENDIX B. Comparing the frictional behavior between the tribo-pin types indicate that friction at the initial stage (0-1 mm sliding distance) is

generally low in the case of uncoated WC-Co cemented carbide pin sliding (Figure 6.4). However, as the steady-state region (1-5 mm of sliding) are reached, a slight increase of friction can be seen. Additionally, the frictional values of uncoated WC-Co cemented carbide tend to fluctuate quite significantly during the end-state (6-10 mm) of the sliding distance, while the friction of the CVD diamond coated pin (Figure 6.5) remains relatively constant over the entire sliding distance after the steady-state region is reached.

Figure 6.4: Frictional sliding curves of WC pins sliding against an as-polished Alumec 89 surface.

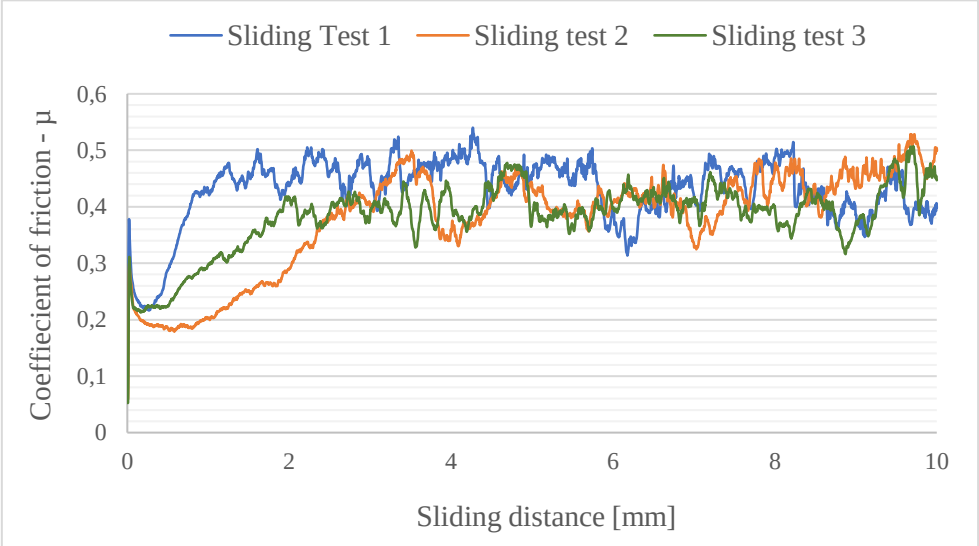

Figure 6.5: Frictional sliding curves of CVD coated pins sliding against an as-polished Alumec 89 surface.

A plotted graph of the average frictional values as a function of sliding distance from all sliding tests are depicted in Figure 6.6. This graph illustrates how the average CoF of both uncoated and CVD diamond coated WC-Co cemented carbide tribo-pins changes over a sliding distance of 10 mm as they are in constant contact with the polished Alumec 89 surface. At the initial stage (0-1 mm) the average friction of all sliding test made by the CVD diamond coated tribo-pin is quite larger compared to the uncoated pin. As each respective pin reach 1 mm of sliding distance, the curves intersect at a frictional value of about 0.36, from which the variation in friction remains relatively constant and similar between both pin types. However, at around 5 mm of sliding, the friction of the uncoated pin begins to deviate towards a value of 0.5, while the friction of the CVD diamond coated pin remains constant at

around 0.4 as sliding continues. Hence, the difference in frictional values during the end-state of sliding is approximately 25 %. Additionally, the friction of the uncoated pin is seen to fluctuate quite significantly towards the very end of the sliding distance.

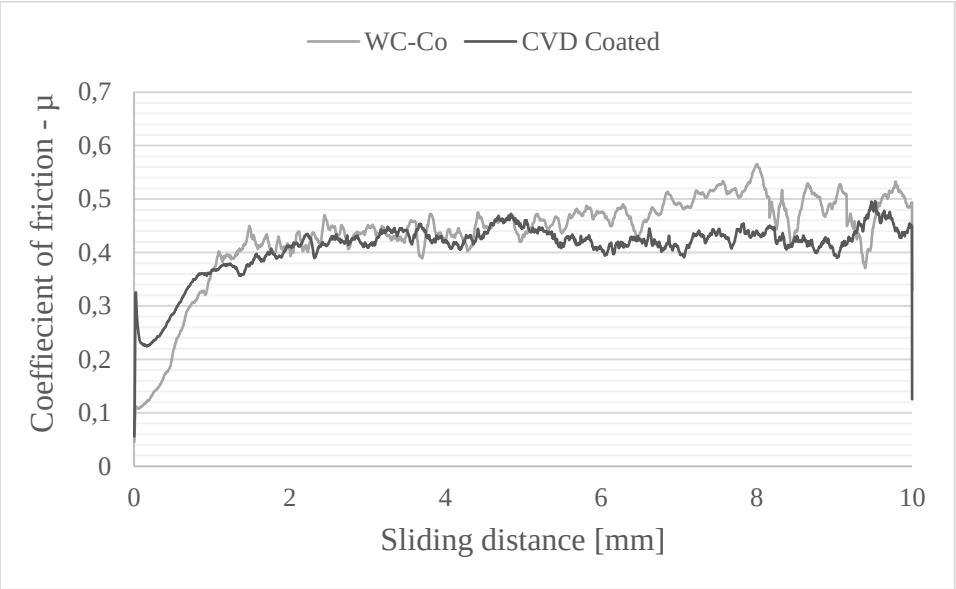

Figure 6.6: Comparison of average CoF as a function of sliding distance for WC-Co cemented caride and CVD pins.

In addition to the graphs shown by Figure 6.6, the average frictional values of the uncoated and diamond coated pins during different stages of the sliding distance are furthermore calculated and presented as bar charts in Figure 6.7. The denotations μ_0, μ_1, μ_2 marks the ranges of sliding distance from which the average frictional value has been calculated. Hence, μ_0 is the average CoF at the initial stage between 0-1 mm. μ_1 is between 1-5 mm and μ_2 is between the final stage of 5-10 mm. From these bar charts it is shown that the average CoF during the end-state of sliding (i.e., in the range denoted by μ_2) is lower (0.43) in the case of CVD diamond coated pin sliding compared with uncoated WC-Co cemented carbide (0.48).

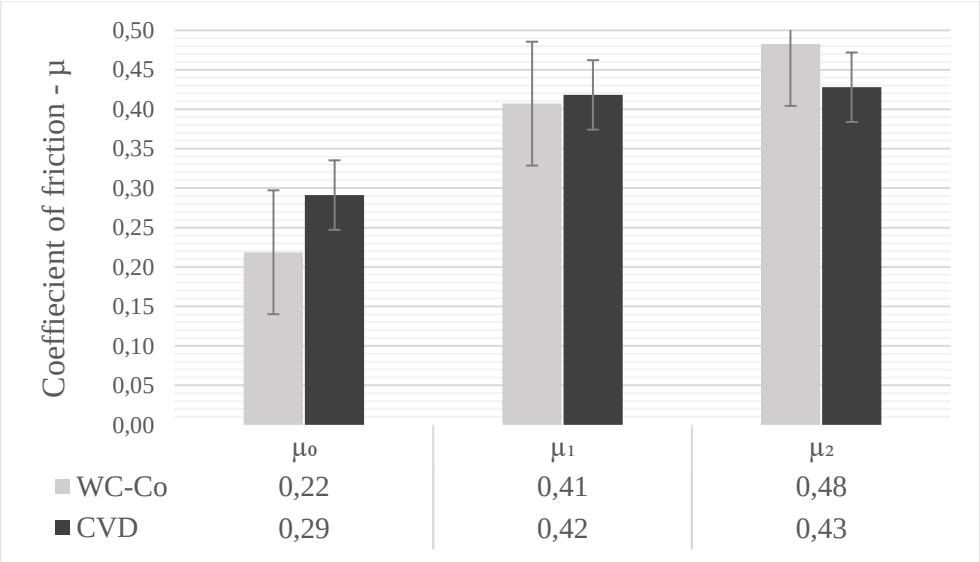

Figure 6.7: Average CoF during different stages of sliding distance.

The regions of pin/surface contact are illustrated in Figure 6.8, in which a comparison regarding adhered aluminum on the uncoated and CVD diamond coated WC-Co cemented carbide pins can be seen. The images depicted are taken of the main area of material interaction, namely at the spherical

region of the pin-tips. During the uncoated pin/surface interaction (Figure 6.8a), BUL formation is characterized as a large black region of transferred aluminum material being adhered onto the grey surface of uncoated WC-Co cemented carbide. Comparing this with the CVD diamond coated pin/surface interaction (Figure 6.8b) reveals a significant difference in BUL formation, where only a small amount of aluminum has been adhered to the respective pin surface.

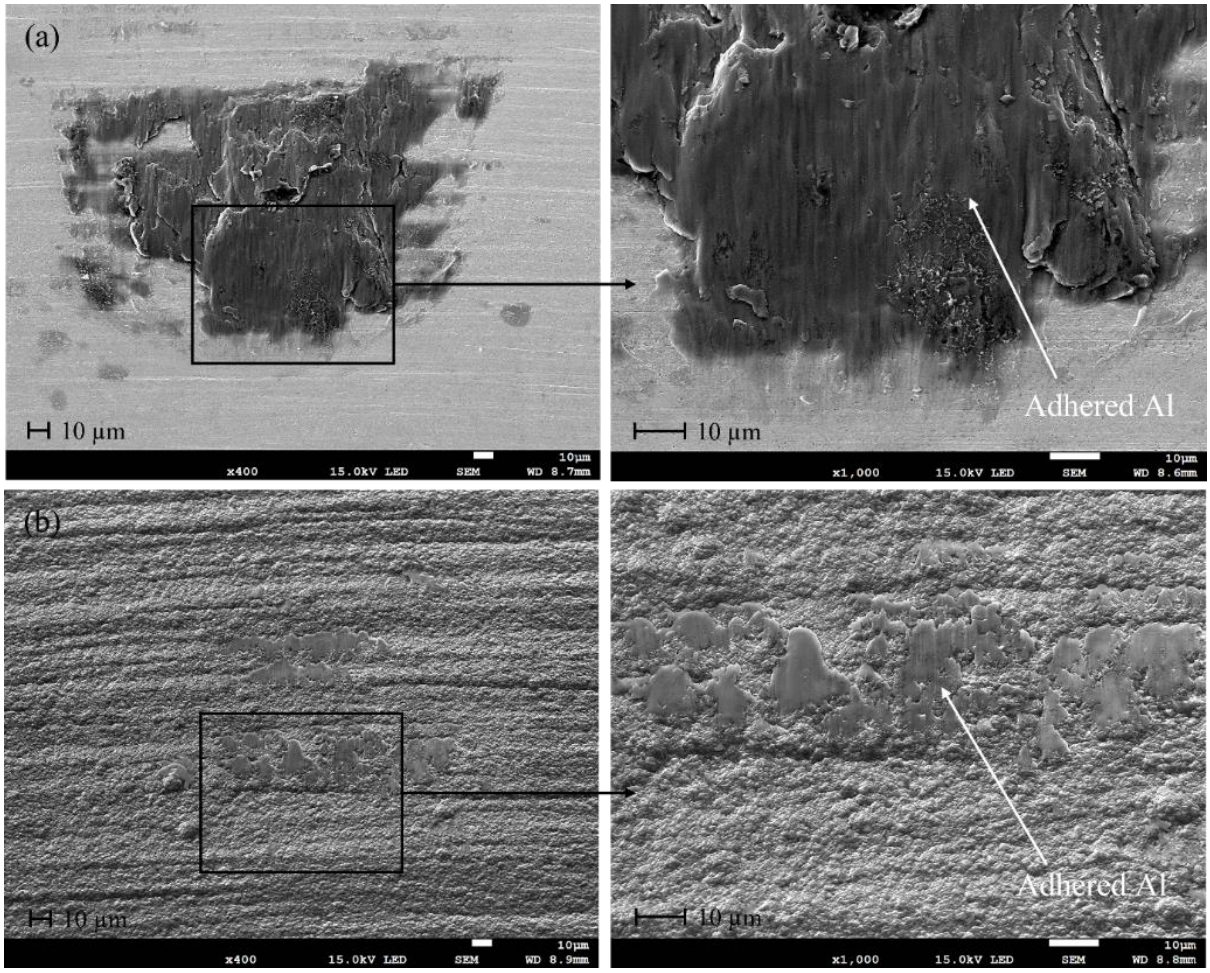

Figure 6.8: Comparison BUL formation on WC vs CVD pin during frictional sliding test. (a) Aluminum BUL on WC pin. (b) Aluminum BUL on CVD coated pin.

Scratch tracks generated during sliding over the as-polished Alumec 89 surface with uncoated and CVD diamond coated pins are presented in Figure 6.9. The images are taken at a position in which the initial running-in period has completed. That is, after about 5 mm of sliding. In the case of uncoated pin sliding, high levels of adhesion are observed due to the evident fractured ridges appearing in the scratch track as illustrated by the enhanced image area of Figure 6.9a. Less adhesive characteristics can be seen in the corresponding scratch tracks generated from the CVD diamond coated pin sliding, as illustrated in Figure 6.9b. In this case, the mechanism of wear seems to be more of an abrasive ploughing action as the pin have slid over the surface. Furthermore, some micro cracking has been initiated as well as wear debris particles remaining in the scratch track.

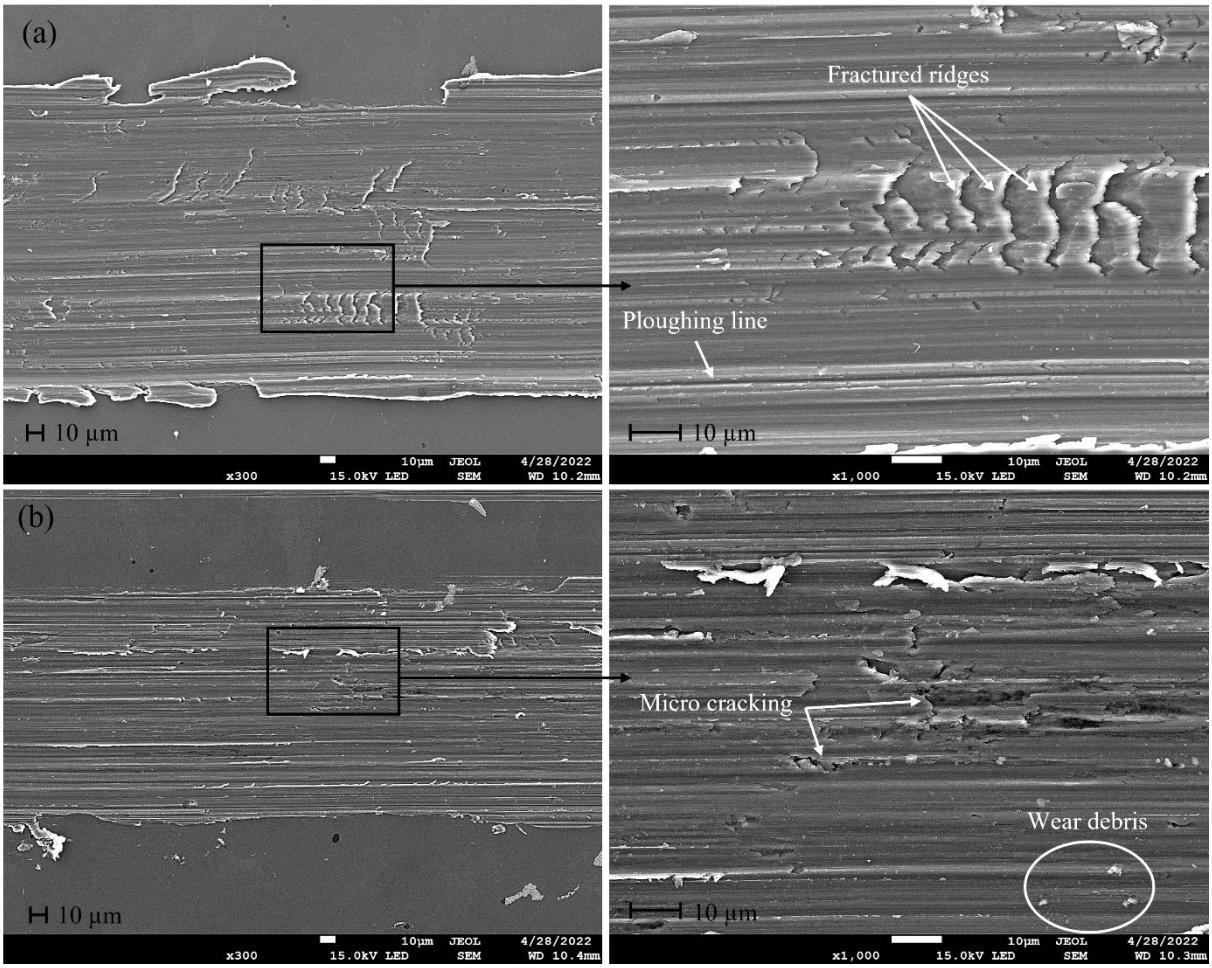

Figure 6.9: Comparison of scratch tracks on polished Alumec 89 surface. (a) Uncoated WC-Co cemented carbide pin scratch track. (b) CVD diamond coated pin scratch track. Please note the more adhesive surface characteristic after the uncoated WC-Co cemented carbide interaction.

6.3 Tribojan pin-turning

Analysis of the uncoated and CVD diamond coated WC-Co cemented carbide tribo-pins used during Tribojan pin-turning tests, as described in section 4.3, are summarized in this paragraph. SEM images of the pins are primarily illustrating characteristics of material transfer resulting from contact interaction between the tribo-pins and the Alumec 89 workpiece bar. Furthermore, the location of the contact interactions observed at the pin surfaces are exemplified in Figure 13.2, APPENDIX B.

The characteristics of material transfer on the uncoated pins are shown by in Figure 6.10. The BUL thickness observed is small and increases as the diameter of the pins become larger. The amount of material transfer are shown to be quite similar during the short time pin-turning tests (Figure 6.10a and c) and seem to increase with contact time duration, as evident by the larger width of the BUL in the long time pin-turning tests (Figure 6.10b and d).

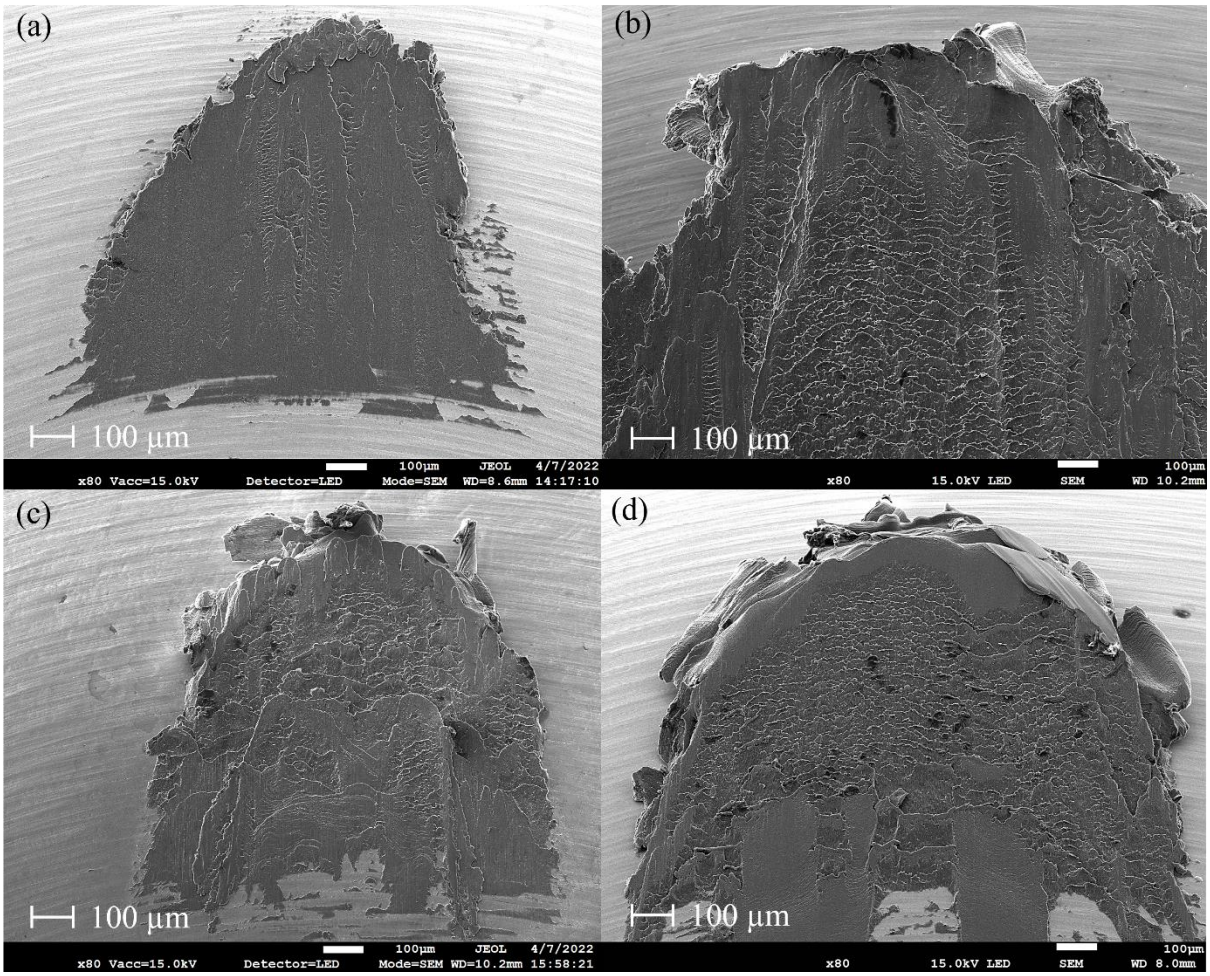

Figure 6.10: Comparison BUL formation on WC-Co cemented carbide pins at different sliding speeds and contact durations. (a) Contact duration 5 s at 600 m/min. (b) Contact duration 30 s at 600 m/min. (c) Contact duration 5 s at 1200 m/min. (d) Contact duration 30 s at 1200 m/min.

The regions of contact between the CVD diamond coated pins and the Alumec 89 workpiece material are illustrated in Figure 6.11. The quality of the diamond coating is observed to be relatively maintained after performed pin-turning tests. Evidence of coating delamination due to wear is not found. The overall diamond growth during the CVD coating process is seen to have evolved in a controlled manner as evident by the still visible grinding marks generated during the machining process of the pins. However, a crack-like feature is shown in the lower left part of Figure 6.11a. This feature was only found on this pin and is probably originating from the grinding process during manufacturing. The thickness of generated BUL: s is observed to be quite thin, as evident by the fact that grinding marks is still visible even in the contact regions between pins and workpiece. Hence, the overall amount of material transfer onto the diamond coated pins is relatively small.

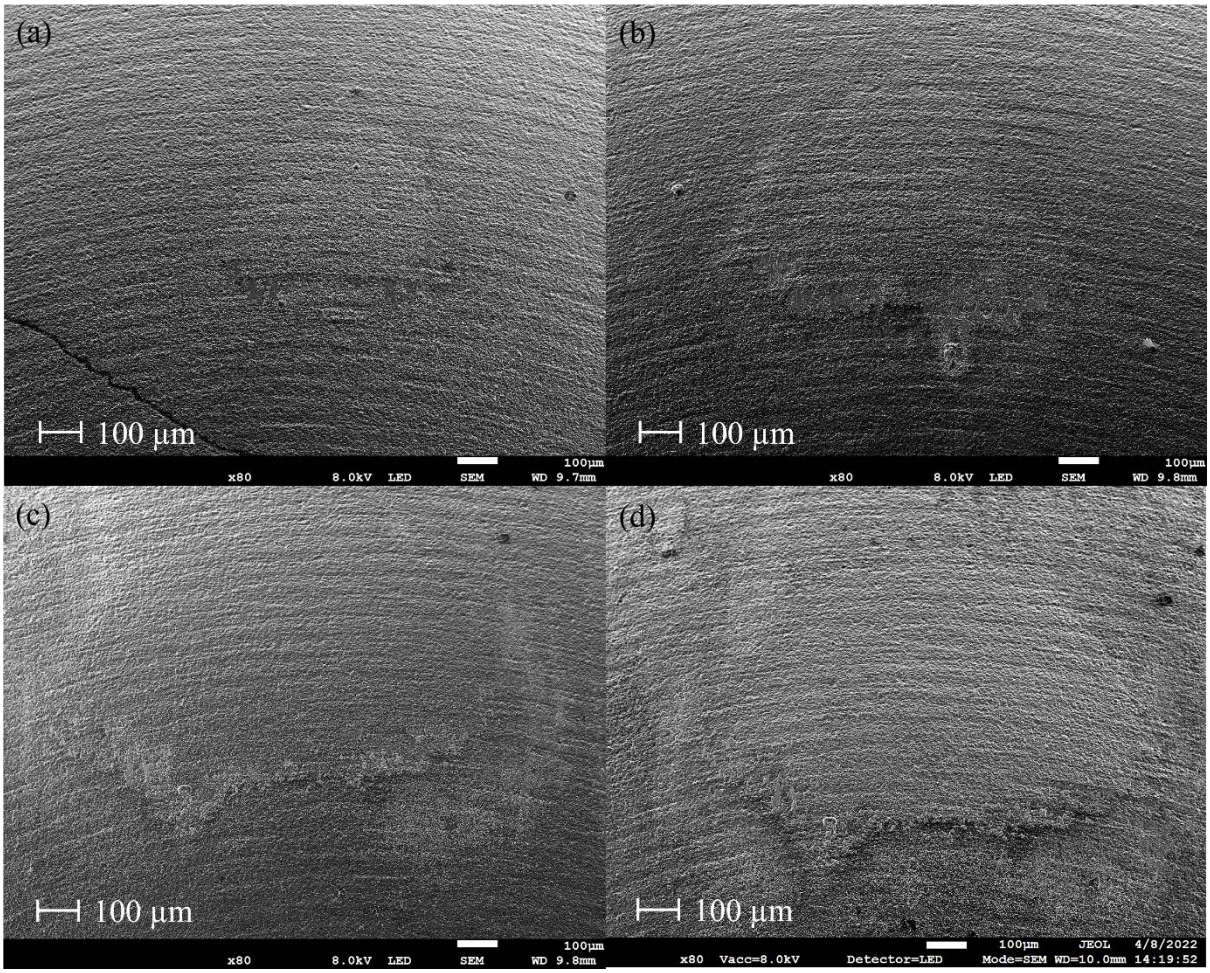

Figure 6.11: Comparison of BUL formation on CVD coated pins at different sliding speeds and contact durations. (a) Contact duration 5 s at 600 m/min. (b) Contact duration 30 s at 600 m/min. (c) Contact duration 5 s at 1200 m/min. (d) Contact duration 30 s at 1200 m/min.

Furthermore, most of the material transfer is seen to be confined in areas closest to the highest point of the pin-tips. As cutting speed and contact time duration increases, the regions of adhered material tend to be more spread out over a broader width of the contact regions. Furthermore, Figure 6.12 illustrates the overall BUL formation generated after pin-turning test of a 30 s pin/workpiece interaction at 1200 m/min sliding speed. The enhanced region of the image is taken in backscatter mode of the SEM, in which the white regions represent accumulation of adhered aluminum on the diamond coated pin-tip. Note that the blob-like feature present in the lower right corner of the image most likely is an artifact from the CVD diamond growth process.

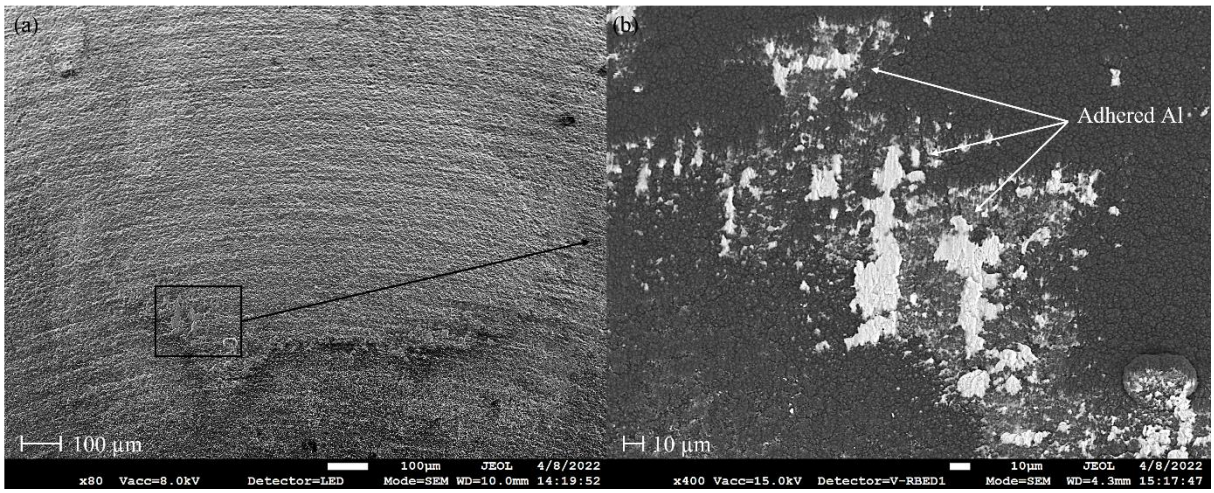

Figure 6.12: Illustration of adhered aluminum at region close to highest point of CVD pin tip. (a) Overview of pin/surface contact at 30 s - 1200 m/min pin turning test. (b) Enhanced region of adhered aluminum taken in backscatter (BS) SEM mode.

Comparison between uncoated and CVD diamond coated WC-Co cemented carbide pins shows quite extensive differences in terms of material transfer. The amount of adhered aluminum onto the uncoated pins after pin-turning are significantly higher compared to the diamond coated pins, as exemplified by Figure 6.10 and Figure 6.11. Additionally, direct comparison made between pins used during a short time contact interaction with low sliding speed, shown by Figure 6.13, indicate high rates of material transfer in the case of uncoated pin interaction with Alumec 89.

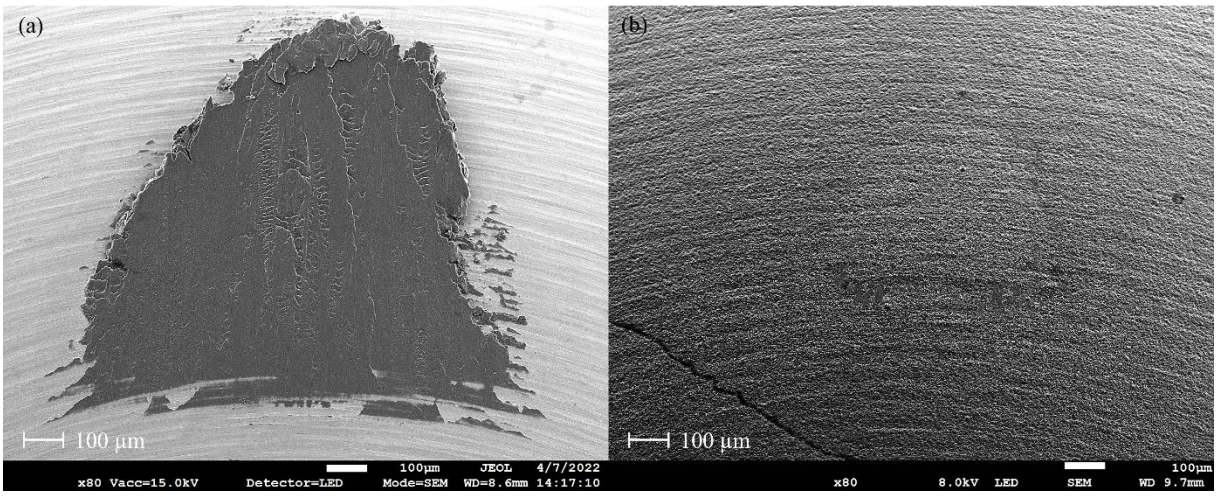

Figure 6.13: Comparison of BUL formation between uniform WC-Co cemented carbide and CVD coated pins. Image (a) and (b) shows BUL formation on uniform WC-Co cemented carbide and CVD coated pins respectively after pin-turning test with 5s contact time duration and 600 m/min cutting speed.

Corresponding sliding tracks generated on the Alumec 89 workpiece surface after pin-turning test with uncoated and CVD diamond coated pins are exemplified in Figure 6.14 and Figure 6.15. The images illustrate pin/surface interactions from pin-turning tests conducted with 5 s contact duration at 600 m/min sliding speed. The surface interaction after pin-turning with the uncoated pin indicates relatively severe adhesive wear at the workpiece surface, as evident by fractured ridges seen in the enhanced image area of Figure 6.14.

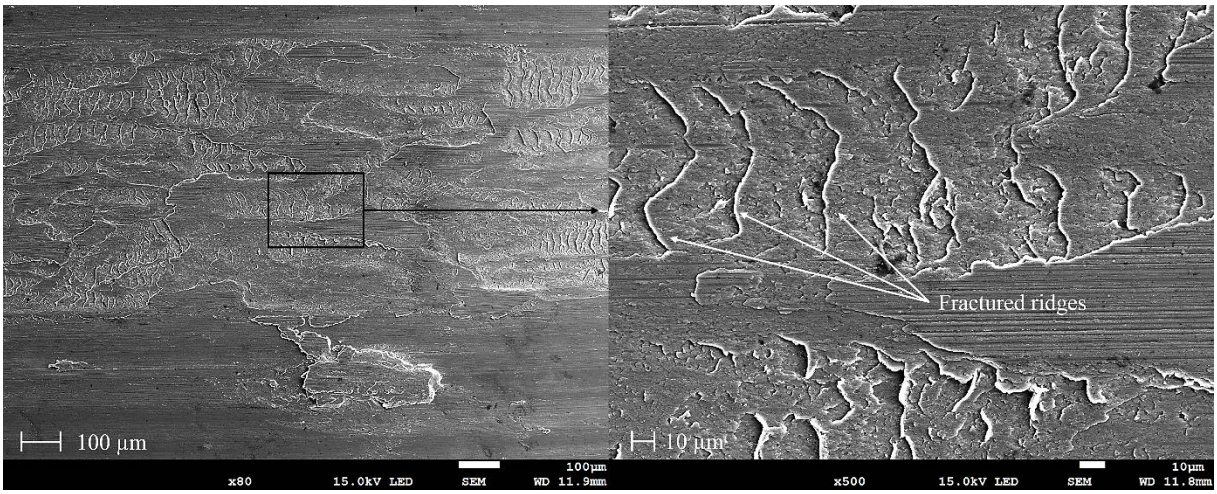

Figure 6.14: Pin/surface interaction between WC-Co pin and Alumec 89 workpiece surface during the 5 s - 600 m/min pin-turning test.

The surface feature produced from the CVD diamond coated pin sliding against the Alumec 89 workpiece, as shown in Figure 6.15, appears to be less severe and more uniformly worn. Additionally, the nature of wear seems to be more abrasive as evident by the horizontal ploughing lines shown in the enhanced image of Figure 6.15. Furthermore, evidence of wear debris is also found in some regions of the worn surface.

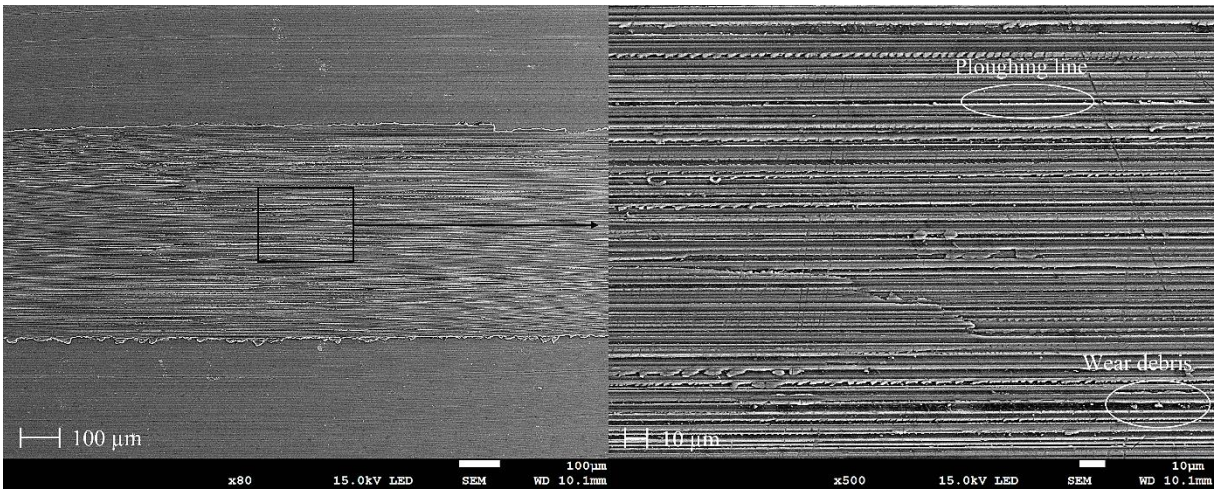

Figure 6.15: Pin/surface interaction between CVD coated pin and Alumec 89 workpiece surface during the 5 s - 600 m/min pin-turning test.

The overall wear behavior of uncoated and diamond coated pins sliding against the workpiece tend to be consistent over all conducted pin-turning tests as shown by Figure 13.3 and Figure 13.4, APPENDIX B. Surface wear produced by the uncoated pins is at its minimum during short time contact interaction at low cutting speed (Figure 13.3a, APPENDIX B). As the duration of contact and sliding speed increases, surface wear is shown to increase. In the case of diamond coated pin/workpiece interaction, the surface wear tend to be more consistent over all pin-turning tests, as illustrated in Figure 13.4, APPENDIX B.

The resulting temperature development near the area of contact during pin-turning, as described in section 4.3, are presented in Figure 6.16. The plotted graphs describe how temperature changes during 30 s long pin-turning operations of uncoated and CVD diamond coated pins, as they interact with the Alumec 89 workpiece surface at a sliding speed of 1200 m/min. Temperature developments of the uncoated and diamond coated pins are represented by the grey and black line respectively. From the appearances of the graphs, the overall temperature development during time of contact is quite similar

between both cases of pin/workpiece interaction. However, the temperature development at the initial state of contact is somewhat higher in the case of uncoated pin/workpiece interaction. As time of sliding progresses the highest temperature generated during this interaction is determined as 47 ºC, as opposed to the diamond coated pin/workpiece interaction which results in a maximum temperature of 42 ºC.

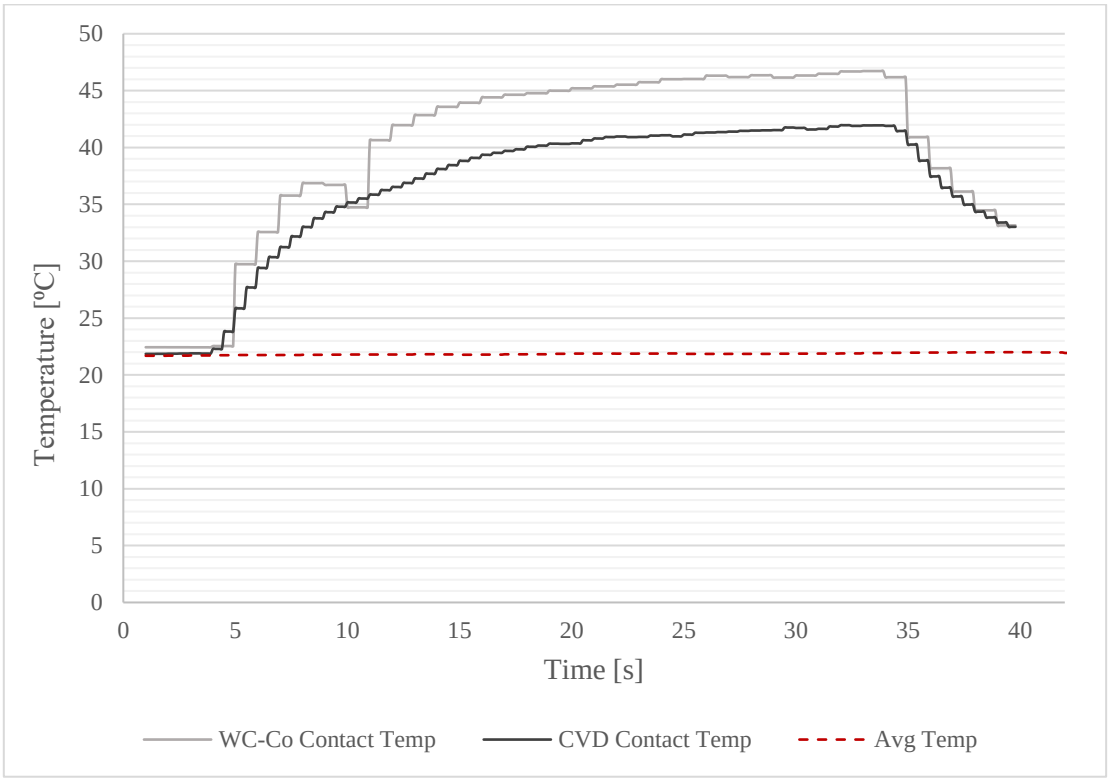

Figure 6.16: Comparison of Tribo-pin contact temperature.

Furthermore, the results from the open pin-turning test are provided by Figure 13.5, APPENDIX B which illustrate spiral sliding tracks generated from an uncoated WC-Co cemented carbide pin sliding against the Alumec 89 workpiece surface. Note how gaps between the sliding tracks is observed due to the feed motion of the lathe machine.

6.4 Longitudinal turning

A comparison of the uncoated WC-Co cemented carbide cutting tools used during the longitudinal turning test, as described in section 4.4, are presented in Figure 6.17. Overviews of the tool edges after machining at different cutting speeds and durations is illustrated. Material transfer, in the form of BUL formation, is observed at the rake face of the tools. The amount of adhered aluminum is seen to be roughly the same in Figure 6.17a, b and c. Furthermore, evidence of material transfer can be seen along the whole cutting-edge after machining of the four evaluated testing conditions. However, a larger amount of BUL-formation at the secondary cutting edge can be observed at a cutting speed of 600 m/min (Figure 6.17a and b). The maximum amount of BUL formation is observed in the case of long workpiece contact duration at high cutting speed (Figure 6.17d). A large chunk of adhered and deformed aluminum is shown to have accumulated within the chip-breaker region, approximately 50-100 µm above the cutting edge of the tool geometry. No significant amount of BUE formation is observed during machining with 600 m/min cutting speed. However, BUE close to the cutting edge of the tools starts to form after 5s of machining at a cutting speed of 1200 m/min. After 60 s of

machining at this cutting speed, a significant amount of adhered aluminum has been transferred onto the flank side of the tool (Figure 6.18).

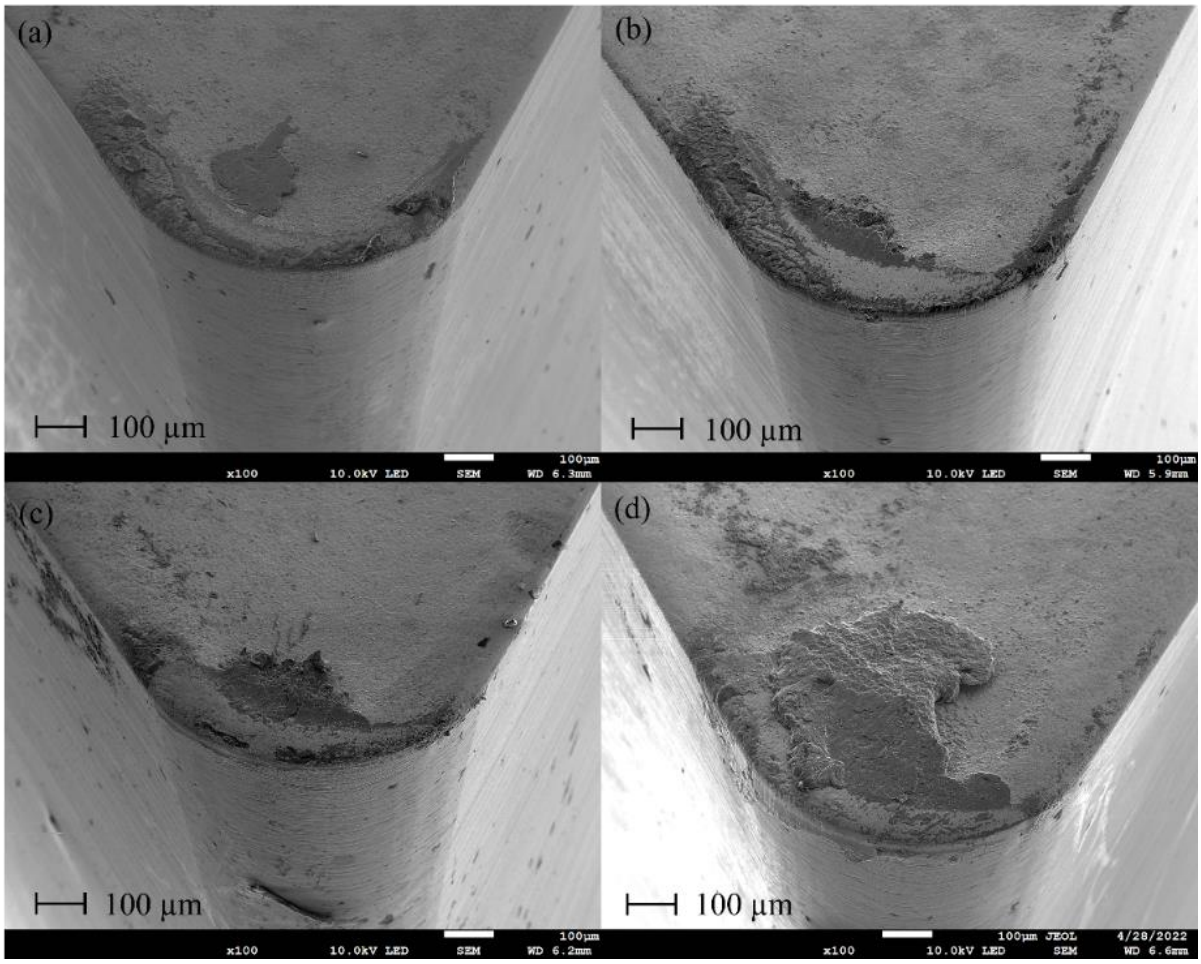

Figure 6.17: Comparison of WC-Co cemented carbide tool inserts used during machining of Alumec 89. (a) Time of cut 5s at 600 m/min. (b) Time of cut 60 s at 600 m/min. (c) Time of cut 5 s at 1200 m/min. (d) Time of cut 60 s at 1200 m/min [26].

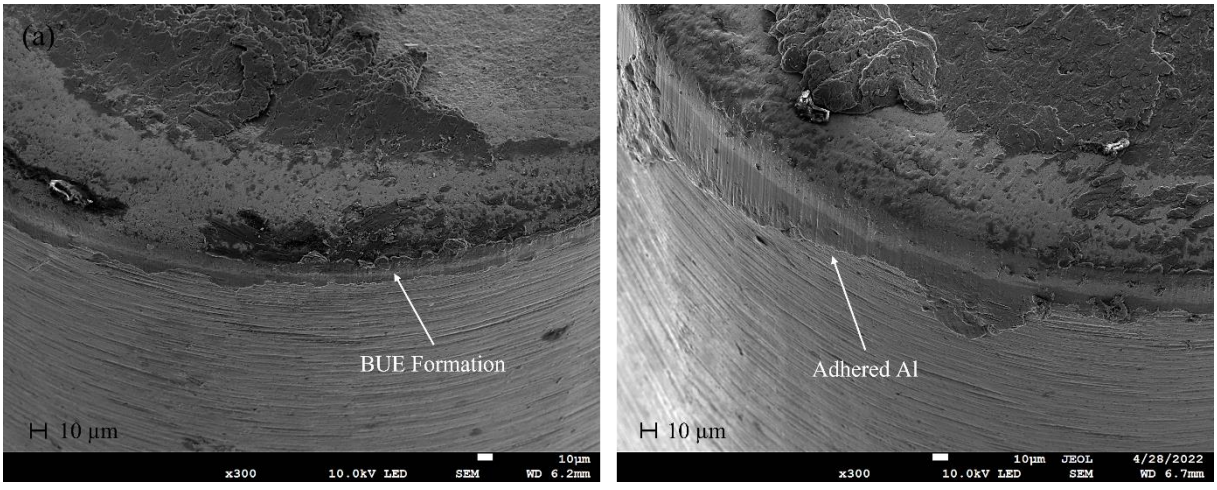

Figure 6.18: Aluminum adherence at flank surface of WC-Co cemented carbide tools at cutting speed 1200 m/min. (a) BUE formation after 5s of continuous machining. (b) Material accumulation of adhered aluminum after 60 s of continuous machining [26].

In a similar manner, comparison of the CVD diamond coated WC-Co cemented carbide cutting tools can be seen in Figure 6.19. Note however that the nose radius of the diamond coated tool inserts are

different than the uncoated ones, which could therefore have some impact on the results. However, the overall BUL formation is seen to be significantly small where some adhered aluminum is observed along the cutting edges of the tools. The characteristic of the BUL: s formed is shown to be both thin and located at small regions along the tool edges.

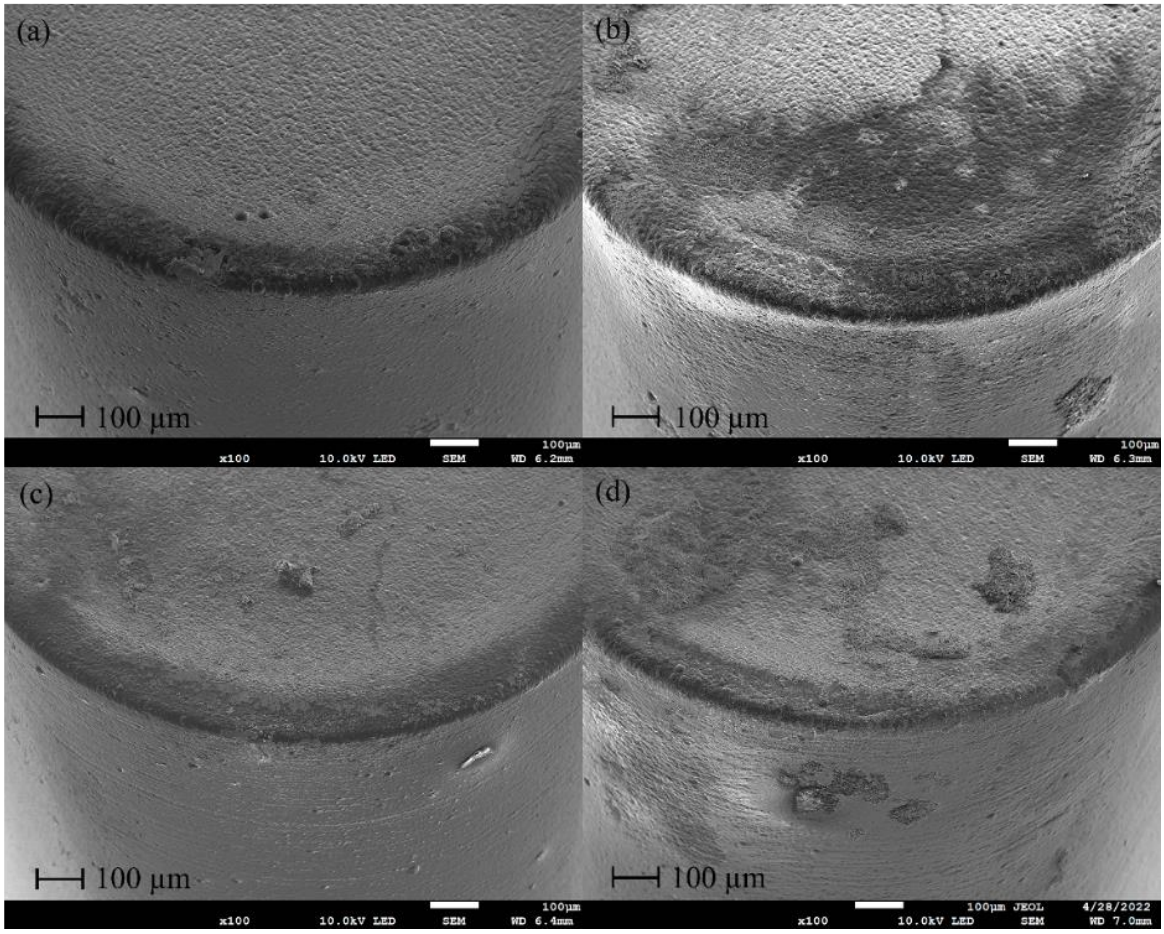

Figure 6.19: Comparison of CVD diamond coated tool inserts used during machining of Alumec 89. (a) Time of cut 5 s at 600 m/min. (b) Time of cut 60 s at 600 m/min. (c) Time of cut 5 s at 1200 m/min. (d) Time of cut 60 s at 1200 m/min [26].

The main characteristics of material transfer formed on the uncoated and CVD diamond coated cutting tools are exemplified in Figure 6.20, where enhanced regions of the cutting edges from the tools used during 60 s of continuous turning at a cutting speed of 1200 m/min is shown. Under these machining conditions, significant amount of adhered Alumec 89 aluminum is observed around the uncoated tool edge, as shown by Figure 6.20a. A thick layer of deformed aluminum has accumulated at the chip-breaker region located approximately 50 µm above the cutting edge. As previously shown, adhered aluminum is also seen along flank face of the tool. However, BUE formation is shown to be relatively small. The characteristics of BUL observed on the CVD diamond coated cutting tool, as shown by Figure 6.20b, reveals that the amount of adhered aluminum is smaller compared to the uncoated tool. The material adherence is more confined closer to the cutting edge, where a small and thin strip of aluminum is seen to have formed on the tool rake face, approximately 40-60 µm above the cutting edge. Furthermore, material adherence is observed on the tool flank face, just below the cutting edge. Note also that some aluminum has adhered in the intersection between the rake and flank face of the tool surface. Similar comparisons of material transfer characteristics from the other tests conducted can be seen in Figure 13.6 - Figure 13.8, APPENDIX B.

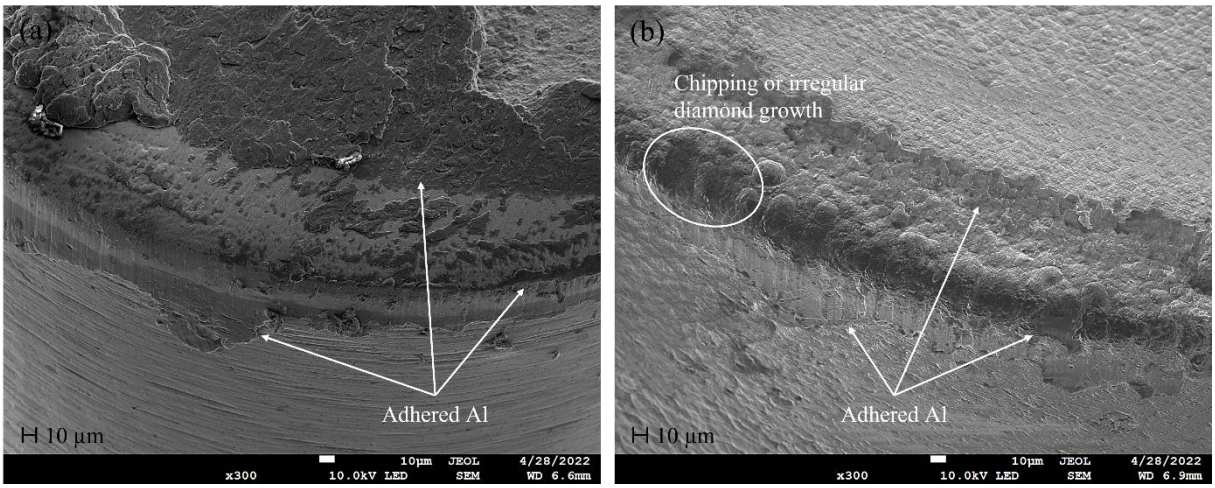

Figure 6.20: Enhanced SEM images of material transfer characteristics at the cutting edges of (a) WC-Co cemented carbide and (b) CVD coated cutting tools [26].

Wear on the CVD diamond coated tools are shown to be close to insignificant. Some indications of eventual chipping at the cutting tool edge can be seen in Figure 6.20b. However, it should be recognized that this feature also could be the result of irregular diamond growth. Furthermore, evidence of both adhesive and abrasive wear is observed during machining with the uncoated WC-Co cemented carbide tools, as exemplified in Figure 6.21.

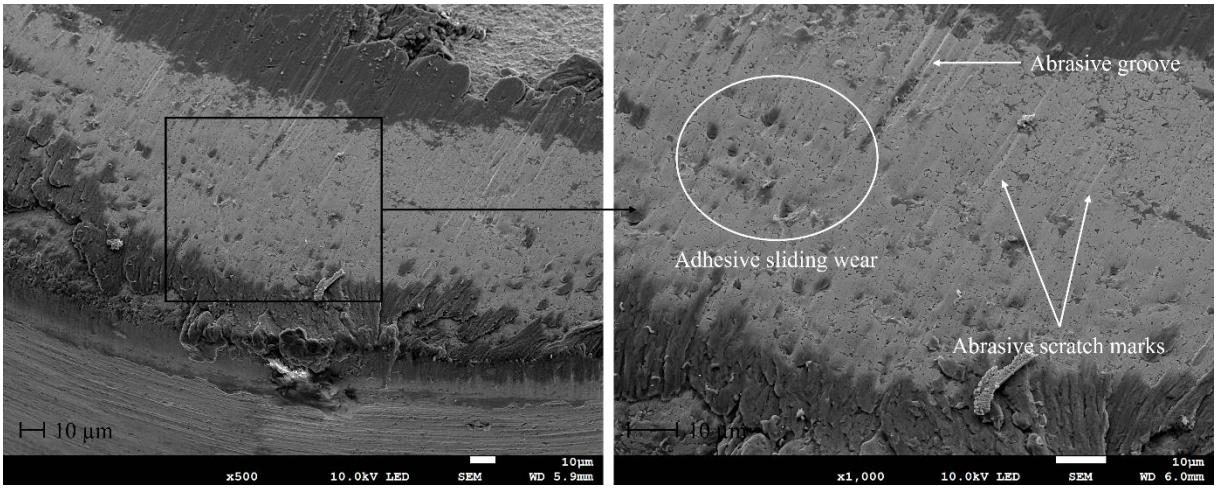

Figure 6.21: Observed wear mechanisms at the rake face of WC-Co cemented carbide tools used during 60 s continuous turning at cutting speed 600 m/min [26].

7 Discussion

The refined tribological properties regarding diamond coated cutting tools used in manufacturing processes of complex nature, such as machining of high-strength aluminum, has been the primary focus of this study. As previously mentioned, the field of tribology is an important topic of consideration in modern product manufacturing. Especially regarding the equipment associated with manufacturing processes of complex nature like machining. The observations made from previous analysis during this project will, in this section, be discussed in a broader perspective as well as provide a summary of the main results gained from all the tests performed.

7.1 Initial observations

Preliminary milling test was conducted during the early stages of the project, with the core purpose of providing some initial knowledge regarding the tribological differences between uncoated and PCD brazed WC-Co cutting tools utilized in milling. After analysis, a relatively large amount of material adherence is observed along the uncoated WC-Co cemented carbide tool edges in milling of both aluminum alloy grades. However, the characteristics of adhered aluminum are shown to be somewhat different. Compared with Alumec 89, machining of the softer and more ductile 6082-grade aluminum results in a more confined and evenly distributed BUL along the edge of the tool. Furthermore, no distinct evidence of BUE is seen, whilst accumulation of adhered aluminum close to the cutting edge is seen in the case of Alumec 89 machining. This behavior could be resulting from differences in mechanical properties of the aluminum alloys (i.e., higher yield strength, hardness, and less ductility of the Alumec 89 alloy). Adhesion against the rake face during chip formation could be stronger in the case of 6082-grade machining, due to the higher ductility of this alloy compared to Alumec 89. Hence, temperature developments in the secondary shear zone would be more evenly distributed which consequently would lead to a more continuous layer of adhered material. Although the characteristics of material transfer is somewhat different, the amount of adhered aluminum at the cutting edges seems to be quite equal when taking the generated BUE seen in Figure 6.1b into account.

Comparing the PCD brazed cutting tools with the corresponding uncoated ones, significant differences is observed in terms of material transfer. No apparent material adherence is seen on the tool rake faces. It is only when reducing the acceleration voltage of the SEM equipment that thin layers of adhered aluminum can be observed. Furthermore, a quite distinct amount of adhered 6082-grade aluminum is observed in and close to the cutting edge in Figure 6.2a. Note also that evidence of chipping wear is observed along the cutting edges of the PCD brazed tools. However, it is possible that this is a result from the manufacturing process of the tools since chipping is observed along the entire tool edges rather than within the areas of contact between the tools and workpieces. These artifacts could have been acting as crack-initiators, which lead to the catastrophic failure just above the tool tip seen in Figure 6.2b. Hence, the combination of improper machining parameters which led to excessive cutting forces, together with chipping along the tool edge finally caused the tool tip failure. An important note is that this type of wear is undesirable in this study since continuous wear during the machining operation is of most importance. However, the result show that effects like these could happen even though relatively ductile materials are being machined.

All in all, it is determined that PCD brazed cutting tools do perform well in terms of material adherence compared to conventional uncoated WC-Co cemented carbide tools. However, due to the brittle nature of the brazed PCD tool tip material, it is important that proper cutting parameters are chosen. This to reduce the risk of excessive crack growth that ultimately could lead to catastrophic failure. Furthermore, the manufacturing costs of PCD brazed tool inserts are high which make them an

expensive alternative for customers, and although PCD tools is an important niche within the industry, commercial use of PCD brazed cutting tools will most likely remain small in the future.

7.2 Frictional aspects of CVD diamond

Frictional sliding tests of the uncoated WC-Co cemented carbide pin revealed similar result in comparison with each other. During the initial state of sliding, the friction is low in all three cases. However, it abruptly increases in a linear fashion until the curves reach a steady-state frictional value of about 0,3-0,5. In the end-state of sliding, a slight increase in friction is observed from the three curves until large fluctuations in frictional values sets in during the very final range of sliding. The corresponding sliding tests conducted using the CVD diamond coated pin indicate that the friction is initially somewhat higher during the initial state compared to the uncoated WC-Co cemented carbide pin. This behavior is probably due to the rougher surface of the coating. Furthermore, the frictional steady-state regime also varies slightly more with the CVD diamond coated pin. However, the level of friction is shown to be lower compared with uncoated WC-Co cemented carbide. It is possible that the steady-state regime of friction is reached at a later stage in this case (i.e., 6 mm of sliding), since the alterations of frictional values seem to become smaller after this point. This observation is in line with previously performed CVD diamond frictional sliding tests, as stated by Najar et al. [4], which mentions that the CoF of microcrystalline diamond (MCD) coatings tend to stabilize at lower values after longer distances of sliding.

The average frictional behavior as a function of sliding distance of uncoated and diamond coated WC-Co cemented carbide pins, as shown by the graphs in Figure 6.6, reveal higher friction at the initial state of sliding with CVD diamond. This behavior could be associated to the surface topography shown in Figure 6.8. The surface of the CVD diamond coated pin is relatively rough compared to the uncoated WC-Co cemented carbide surface. Hence, the ploughing component μ_p would intuitively be the governing factor in the case of CVD diamond. During the steady-state regime (i.e., between 2-5 mm of sliding), frictional values of both materials are almost equal. However, the friction of WC-Co cemented carbide is shown to both increase and alternate significantly, whilst the friction of CVD diamond remains at similar values during both the steady-state regime and the final range of sliding. Hence, the frictional properties of CVD diamond in contact with Alumec 89 are indicated to be good whilst the frictional values of WC-Co cemented carbide tend to increase over longer distances of sliding. Additionally, when studying the scratch tracks generated on the as-polished Alumec 89 surface, indications of pronounced adhesive wear is observed in the case of uncoated WC-Co cemented carbide pin sliding. In the case of CVD diamond coated pin sliding, ploughing lines seem to be more frequent which would indicate that the adhesion is weaker during the contact interaction. These frictional characteristics are further enhanced when studying the pin/surface interactions during the Tribojan pin-turning tests.

7.3 Characteristics and mechanisms of material transfer

When analyzing the results gathered from the frictional sliding test, it is obvious that the difference in material transfer is significant between uncoated and CVD diamond coated WC-Co cemented carbide surfaces during interaction with high-strength Alumec 89 aluminum. Adherence of aluminum onto the uncoated WC-Co cemented carbide surface is relatively high even at low normal loads and sliding speeds compared to the CVD diamond coated surface. Additionally, adhered aluminum appears to have been built up in the whole area of contact, whilst material adherence seems to be confined in smaller regions in the case of CVD diamond coated interaction with Alumec 89. This behavior is also recognized during the Tribojan pin-turning tests. The area of contact during pin-turning with uncoated

WC-Co cemented carbide pins are clearly recognizable when studying Figure 6.10. Furthermore, the amount of BUL formation seems to have somewhat higher dependence with contact time rather than rotational speed, since the width of adhered material is larger during the two 30 s pin-turning tests. On the other hand, material transfer onto the CVD diamond coated pins appear to be significantly thinner and more distinguished along the edges of the pin/surface contact. The difference in BUL thickness between uncoated and CVD diamond coated WC-Co cemented carbide is further emphasized by the fact that grinding marks in the contact area are still visible after pin-turning with CVD diamond coated pins. Furthermore, most of the visible aluminum being adhered tend to be confined close to the top of the CVD diamond coated pins.

As for the frictional test, the surface topography from a ploughing point of view should result in more material transfer for the CVD diamond coated pins. However, the results show the opposite since adhesion instead is shown to be low. To explain this observation, the topics of surface structure and frictional characteristics are revisited. As mentioned, the structure of CVD diamond coated pin surfaces appears to be somewhat rougher compared to the uncoated WC-Co cemented carbide pins. Hence, the friction should be higher. However, the adhesion between CVD diamond and Alumec 89 appears to be weaker compared with uncoated WC-Co cemented carbide. This would therefore imply that the frictional adhesion component μ_a is larger in the case of uncoated WC-Co cemented carbide, which indirectly would lead to the higher temperature development in the contact-zone, as also shown by Figure 6.16. Furthermore, diamond is recognized as being relatively inert and do not react with aluminum at all. On the other hand, the Co present in WC-Co cemented carbide shows higher tendencies of reacting with aluminum, which further results in a higher adherence. This fact is further underlined when studying the phase diagrams of C-Al and Co-Al systems respectively. Examples of these are given by Figure 13.9 and Figure 13.10, APPENDIX B. Taking this into account, together with the fact that the initial tribo-film formation is a chemically induced process [8], chemical reactions in the contact interface should be more easily initiated during uncoated WC-Co cemented carbide interaction with Alumec 89. Hence, the difference of temperature developments in the contact-zones during uncoated and CVD diamond coated WC-Co cemented carbide pin-turning, along with their respective chemical properties and frictional characteristics, could give a possible explanation to the differences observed regarding material transfer. However, it should be recognized that the temperature measurements preformed in this study were rather simplistic in its nature and developed as an attempt to only acquire indications of contact-zone temperature developments. The measurements were made in an area a few millimeters from the real contact-zone. Furthermore, only a few measurements were made, which provided low statistical accuracy. Due to these aspects, the temperature results should be considered as indications. The actual contact-zone temperature is more likely to be in the ranges of 200 °C or more. Especially when regarding high-speed turning [27].

The rate of material transfer is shown to be relatively high in the case of uncoated WC-Co cemented carbide pin-turning. Hence, possible wear mechanisms at the surface of the pins are difficult to determine due to the extensive adherence of aluminum. Therefore, further investigations regarding underlying wear mechanisms are recommended. However, in the case of CVD diamond coated pin-turning, no significant wear has been observed. The only implication of the pin-turning tribo-pair interaction, in terms of surface morphology, are shown to be material transfer.

7.4 Tribological implication in longitudinal turning

The results acquired and observed from the refined tribological tests tend to also occur in actual longitudinal turning operations. Significant amounts of aluminum adherence are observed along and around the cutting edges of the uncoated WC-Co cemented carbide tools used during turning. During all machining conditions in this study, adhered aluminum is observed along the whole cutting edges of

the tools used. Furthermore, accumulation of aluminum within the so-called chip-breaker region of the tools is visible during all tests performed. Additionally, the accumulation seems to be more pronounced at long term tool/workpiece interactions at higher cutting speeds. This is somewhat counterintuitive to the corresponding results of uncoated WC-Co cemented carbide pin-turning, since the time of contact interaction seemed to have larger influence on the amount of aluminum adherence, rather than cutting speed. However, these observations might be the result of geometrical differences between cutting tools and tribo-pins since the appearance of the BUL: s between the tests are similar.

As shown by the results given from the refined tribological tests, the tendencies of aluminum material transfer onto CVD diamond coated surfaces are significantly less compared to uncoated WC-Co cemented carbide. This result is in line with observations made by Chattopadhyay et al. [28], which recognized that there was essentially no trace of BUE formation on CVD diamond coated tool inserts after machining of aluminum. Similar observations are also shown during the longitudinal turning operations made in this study. Some adhered aluminum is present at the tool rake faces of the CVD diamond coated tools. However, the amount in terms of thickness and distributed area is significantly smaller compared to the uncoated WC-Co cemented carbide tools. Note also that the characteristics of BUL: s at the rake faces shown in Figure 6.20 are quite like those observed from the frictional and pin-turning tests. When regarding wear, the effects on both cutting tool types are shown to be relatively small. In fact, wear at the CVD coated tool surface is close to insignificant. This result is in line with statements made by Santos et al. [1], which correlates the low chemical affinity of diamond to improved machinability of aluminum. The features of some regions at the cutting edge might be recognized as micro chipping, as exemplified in Figure 6.20b. However, these features could also be the result of irregular diamond growth during the CVD process. Furthermore, wear at the uncoated WC-Co cemented carbide tool faces is also recognized as small. Some abrasive grooves and scratch tracks in the chip flow direction are detected at the tool rake faces, which do give indications of abrasive wear mechanisms being present during the turning operation. Hard precipitants or intermetallic phases in Alumec 89 could be one possible reason for this. However, these are significantly small and should not be able to cause the abrasive wear marks observed at the tool rake face. It is more likely that some other rare types of hard particles are formed during the turning operation. Note that this statement should be considered as speculation since no closer investigation of hard particle formation was conducted in this study. Furthermore, evidence of adhesive sliding wear is also observed at the uncoated WC-Co cemented carbide tool, which could be the result of the adhesive tendencies (i.e., frictional and surface characteristics of uncoated WC-Co cemented carbide) seen during the refined tribological tests.

8 Conclusion

The main conclusions made from the experimental studies and micrographic analysis of the refined tribological characteristics regarding CVD diamond is summarized and presented in this section.

1. The average CoF of CVD diamond interacting with the aluminum alloy Alumec 89 is shown to be generally lower (0.43) compared to WC-Co cemented carbide (0.48). Furthermore, the frictional behavior and characteristic of CVD diamond appears to be more consistent and regular over longer sliding distances.

2. Contact interaction between CVD diamond and Alumec 89 appears to be of abrasive nature due to the rough surface structure of the diamond coating, whilst the corresponding tribo-pair contact interaction with uncoated WC-Co cemented carbide shows more adhesive tendencies.

3. Temperature developments in the contact-zone during pin-turning appears to be lower in the case of CVD diamond.

4. CVD diamond are shown to perform well in terms of material transfer characteristics when interacting with high-strength aluminum. The amount of material adherence is observed to be significantly reduced on CVD diamond coated surfaces.

5. Tribological characteristics generated during the closed Tribojan pin-turning tests are shown to be transferable to actual machining, which indicate that the testing method performs relatively well as compliment to conventional frictional sliding and machining testing.

6. No significant evidence of wear is observed on CVD diamond coated cutting tools used during continuous longitudinal turning. However, both adhesive and abrasive wear mechanisms seem to be acting during turning with conventional uncoated WC-Co cemented carbide cutting tools.

9 Further work

Much of the frictional aspects regarding the CVD diamond coated as well as uncoated WC-Co cemented carbide surface interactions with Alumec 89 was determined using traditional scratch/sliding test method. However, this method is conducted under very controlled conditions, with poor resemblance to actual machining. One way of resolving this issue could be to incorporate strain gauges with the Tribojan equipment to provide the ability of frictional measurements during pin-turning testing. This would increase the flexibility of the Tribojan, as well as reducing the gap between controlled laboratory conditions and actual machining. Further knowledge about the refined tribological properties of CVD diamond coated tools used in metal cutting could therefore possibly be gained.

This master thesis project has systematically shown that the degree of material transfer (i.e., aluminum adherence) onto CVD diamond coated surfaces is low compared to uncoated WC-Co cemented carbide surfaces. However, the underlying chemical processes during surface contact has not yet been investigated and detailed analysis regarding initial tribo-film formation should therefore be considered. This could be achieved by utilizing the so-called focused ion beam (FIB) technique to produce high-quality cross-sectional cuts of the test samples, which further allow for detailed microscopic analysis of the interface between adhered aluminum and the cutting tool substrate material. Furthermore, the FIB technique could also be incorporated together with SEM analysis to gain knowledge regarding any possible graphitization of diamond during machining. This would be an interesting topic of research, since graphitization would favor low frictional values of diamond.

Although CVD diamond coated cutting tools are shown to perform well in terms of material transfer and tribo-film formation, the diamond growth process is still quite difficult to manage and control, as evident by the rough surfaces structures produced as a result from the CVD process. From a tribological point of view, diamond growth irregularities at the surfaces of CVD diamond coated cutting tools could result in reduced surface finish of the final product after machining. Hence, increasing the knowledge about the diamond growth process would be an area of interest as to further improve the CVD coating of the cutting tools. Furthermore, the interfacial strength between CVD coating and WC-Co cemented carbide substrate have been shown to be problematic due to presence of cobalt. Hence, further research should be done to reduce the risk of coating delamination during, especially, long-time machining.

10 Acknowledgements

First and foremost, I would like to thank my classmate and project colleague Oskar Lundquist for all the assistance and support given throughout this project as well as our years of studies together. It has truly been a pleasure and I hope that we will get the opportunity of working together again sometime in the future.

A special thank you also goes to my supervisor, Mikael Fallquist at Karlstad University, for providing the opportunity of conducting this master thesis, as well as the precise and constant guidance given throughout the duration of the project. Your insights and knowledge regarding the subject of tribology along with your positive attitude has been of huge importance during this exciting journey.

Many thanks to the team at SECO Tools AB in Fagersta Sweden, including Rachid M'Saoubi, Per Alm and Lennart Karlsson. Your collected expertise and experience within both the industrial and scientific fields of research have been of immense value during this thesis project. Furthermore, I also would like to acknowledge and thank Jesper Blomgren and Erik Furia at SECO Tools testing and research facility for producing such fine research material for both mine and Oskars thesis projects. You truly made our visit at SECO Tools AB especially fun and fruitful.

Finally, I would also like to thank Lars Holm at the Karlstad University workshop for all support given during the project. Your insights regarding workshop manufacturing, as well as your positivity and curiosity, has been of tremendous importance during this thesis project. Furthermore, your constant will to help have also been a key factor in the sense of keeping the work continuously moving forward throughout the duration of the project.

11 Bibliography

[1] M. C. Santos Jr, A. R. Machado, W. F. Sales, M. A. S. Barrozo och E. O. Ezugwu, ”Machining of aluminum alloys: a review,” *Int J Adv Manuf Technol,* vol. 86, pp. 3067-3080, 2016.

[2] M. Fallquist, ”Microstructural, Mechanical and Tribological Characterization of CVD and PVD Coatings for Metal Cutting Applications,” Uppsala University, Uppsala, 2012.

[3] D. Jianxin, Z. Hui, W. Ze, L. Yunsong och Z. Jun, ”Friction and wear behaviours of WC/Co cemented carbide tool materials with different WC grain sizes at temperatures up to 600 C,” *Int. Journal of Refractory Metals and Hard Materials,* vol. 31, pp. 196-204, 2012.

[4] K. A. Najar, N. Sheikh, M. M. Butt, S. Mushtaq och M. Shah, ”Engineered Synthetic Diamond Film as a Protective Layer for Tribological and Machining Applications: A Review,” *Journal of Bio- and Tribo-Corrosion,* vol. 5, nr 59, pp. 1-16, 2019.

[5] I. Hutchings och P. Shipway, TRIBOLOGY: Friction and Wear of Engineering Materials (Second Edition), Oxford: Elsevier Ltd, 2017.

[6] C. R. Gagg och P. R. Lewis, ”Wear as a product failiure mechanism - Overview and case studies,” *Engineering Failure Analysis,* vol. 14, pp. 1618-1640, 2007.

[7] I. C. Engin, ”Theories on Rock Cutting, Grinding and Polishing Mechanisms,” IntechOpen Limited, 08 05 2012. [Online]. Available: https://www.intechopen.com/chapters/44462. [Använd 16 03 2022].

[8] S. Jacobson och S. Hogmark, ”Tribofilms - On the crucial importance of tribologically induced surface modifications,” Uppsala University, Uppsala, 2010.

[9] H. Johannesson, J.-G. Perssom och D. Pettersson, Produktutveckling - Effektiva metoder för konstruktion och design, Stockholm: Liber AB, 2013.

[10] M. E. Merchant, ”Mechanics of the Metal Cutting Process. 1. Orthogonal Cutting and a Type 2 Chip,” *Journal of Applied Physics,* vol. 16, nr 5, pp. 267-275, 1945.

[11] E. Tóth-Laufer och R. Horváth, ”Fuzzy model based surface roughness prediction of fine turning,” *FME Transactions,* vol. 45, pp. 181-188, 2017.

[12] S. Jacobson och P. Wallen, ”A NEW CLASSIFICATION SYSTEM FOR DEAD ZONES IN METAL CUTTING,” *Int. J. Mach. Tools Manufact.,* vol. 28, nr 4, pp. 529-538, 1988.

[13] T. Dursun och C. Soutis, ”Recent developments in advanced aircraft aluminum alloys,” *Materials and Design,* vol. 56, pp. 862-871, 2014.

[14] J. García, V. C. Ciprés, A. Blomqvist och B. Kaplan, ”Cemented carbide microstructures: a review,” *International Journal of Refractory Metals & Hard Materials,* vol. 80, pp. 40-68, 2019.

[15] A. Inspektor, E. J. Oles och C. E. Bauer, ”Theory and Practice in Diamond Coated Metal-Cutting Tools,” *Int. J. of Refractory Metals & Hard Materials,* vol. 15, pp. 49-56, 1997.

[16] T. A. Scott, ”The influence of microstructure on the mechanical properties of polycrystalline diamond: a literature review,” *Advances in Applied Ceramics,* vol. 117, nr 3, pp. 161-176, 2017.

[17] G. Li, M. Z. Rahim, W. Pan, C. Wen och S. Ding, ”The manufacturing and application of polycrystalline diamond tools - A comprehensive review,” *Journal of Manufacturing Processes,* vol. 56, pp. 400-416, 2020.

[18] H. Liu och D. S. Dandy, ”Diamond CVD Techniques,” i *Diamond Chemical Vapor Deposition - Nucleation and Early Growth Stages*, 1995, pp. 14-45.

[19] Unknown, ”Tribonet,” Tribonet-About tribology, [Online]. Available: https://www.tribonet.org/tribometer/. [Använd 25 03 2022].

[20] J. Sekler och H. E. Hintermann, ”The scratch test: Different critical load determination techniques,” *Surface and Coatings Technology,* vol. 36, nr 1-2, pp. 519-529, 1988.

[21] N. M. Jennett och S. Owen-Jones, ”The Scratch Test: Calibration,Verification and the Use of a Certified Reference Material - Measurement Good Practice Guide No 54,” NPL Materials Centre, London, 2002.

[22] M. Olsson, B. Stridh, S. Söderberg och U. Jansson, ”Sliding wear of hard materials - the importance of a fresh countermaterial surface,” *Wear,* vol. 124, nr 2, pp. 195-216, 1988.

[23] F. Schultheiss, M. Fallquist, R. M’Saoubi, M. Olsson och J.-E. Ståhl, ”Influence of the tool surface micro topography on the tribological characteristics in metal cutting - Part 2 Theoretical calculations of contact conditions,” *Wear,* Vol. %1 av %2298-299, nr 1, pp. 23-31, 2013.

[24] J. E. Stahl, Metal Cutting Theories and Models, Division of Production and Materials Engineering, 2012.

[25] Y. Leng, Materials Characterization: Introduction to Microscopic and Spectroscopic Methods - Second Edition, Weinheim: Wiley-VCH, 2013.

[26] O. Lundquist, ”Wear of CVD diamond coated tools during machining of high strength aluminum alloy,” Karlstad University, Karlstad, 2022.

[27] D. Biermann och M. Kirschner, ”New coating systems for temperature monitoring in turning processes,” *Surface & Coatings Technology,* vol. 215, pp. 376-380, 2013.

[28] A. K. Chattopadhyay, P. Roy, A. Ghosh och S. K. Sarangi, ”Wettability and machinability study of pure aluminum towards uncoated and coated carbide cutting tool inserts,” *Surface and Coatings Technology,* vol. 203, nr 8, pp. 941-951, 2009.

[29] R. Dabouz, M. Bendoumia, L. Belaid och M. Azzaz, ”Dissolution of Al 6%wt C Mixture Using Mechanical Alloying,” *Defect and Diffusion Forum,* vol. 391, pp. 82-87, 2019.

[30] M. Noori och B. Hallstedt, ”Thermodynamic modelling of the Al-Co-Mn system,” *Calphad: Computer Coupling of Phase Diagrams and Thermochemistry,* vol. 71, pp. 1-13, 2020.

12 APPENDIX A

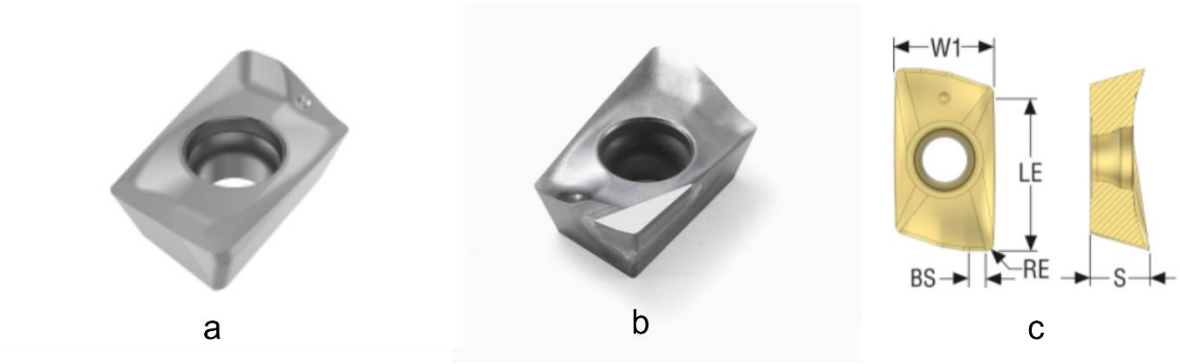

Figure 12.1: Cutting tool geometry description. a) homogeneous WC-Co cemented carbide insert. b) PCD brazed cemented carbide insert. c) geometric cutting tool features.

Table 12.1: Geometric values regarding cutting tool features of WC-Co cemented carbide and PCD brazed cemented carbide inserts.

Type	W1 [mm]	LE [mm]	BS [mm]	RE [mm]	S [mm]
WC-Co	8,2	12,0	1,6	0,80	5,03
PCD	8,2	4,0	1,1	0,40	5,03

Table 12.2: Machining parameters regarding preliminary milling tests

Parameter description	Unit value
Cutting speed [m/min]	600
Feed Rate [mm/min]	0,3
Cutting depth [mm]	1
Engagement [%]	30

Table 12.3: Description of workpiece and tool insert combinations, as well as number of passings over the respective workpiece surface.

Combination of workpiece material and cutting tool insert	Number of passings over the 150 mm workpiece surfaces
Alumec 89 - WC-Co	1
Alumec 89 - WC-Co	10
Al 6082 - WC-Co	1
Al 6082 - WC-Co	10
Alumec 89 - PCD	10
Al 6082 - PCD	10

Table 12.4: Description of parameter settings and conditions regarding the Tribojan pin-turning method with static tribo-pin motion.

Test nr	Pin-material	Cutting speed [m/min]	Contact time [s]
1	WC-Co	600	5
2	WC-Co	600	30
3	WC-Co	1200	5
4	WC-Co	1200	30
5	CVD coated	600	5
6	CVD coated	600	30
7	CVD coated	1200	5
8	CVD coated	1200	30

Table 12.5: Performance data of Okuma SPACETURN LB4000 EX II CNC lathe machine.

Parameter description	Unit value
Max. turning diameter [mm]	480
Max. turning length [mm]	380
Spindle speed [min^{-1}]	4200

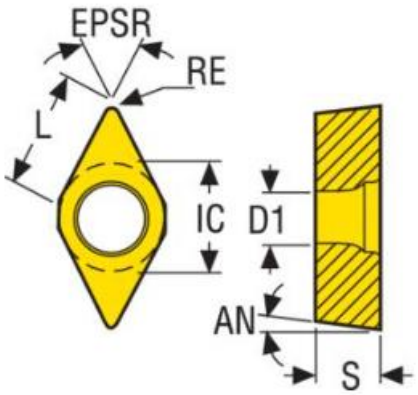

Figure 12.2: Geometric description of cutting tool inserts used in longitudinal turning tests.

Table 12.6: Geometric values for cutting tool inserts used in longitudinal turning tests.

Insert type	WC-Co	CVD	PCD
Seco code	DCGT11T304-M3 HX	DCGT11T308-M3 HX	DCMW11T304F-L1 PCD20
L [mm]	11.60	11.60	11.60
EPSR [deg]	55.0	55.0	55.0
RE [mm]	0.40	0.80	0.40
IC [mm]	9.53	9.53	9.52
D1 [mm]	4.5	4.5	-
AN [deg]	7.0	7.0	7.0
S [mm]	3.97	3.97	3.97

Table 12.7: Unit descriptions regarding cutting tool insert geometry.

Geometric unit description	**Name**
Theoretical cutting-edge length	L
Cutting angle	EPSR
Corner radius	RE
Circle diameter	IC
Mounting diameter	D1
Clearance angle	AN

Table 12.8: Longitudinal turning test matrix.

	Time (s):	60				5		
	Materials:	WC-Co	CVD	PCD		WC-Co	CVD	PCD
Cutting speeds:								
1200 m/min		3	3	3		3	3	0
900 m/min		3	3	0		3	3	0
600 m/min		3	3	1		3	3	0

Constant cutting parameters

Depth of cut	0,5 mm
Feed rate	0,1 mm/rev

Total samples: 40

Figure 12.3: Illustration of manufactured sample holder used during SEM analysis of cutting tool inserts.

13 APPENDIX B

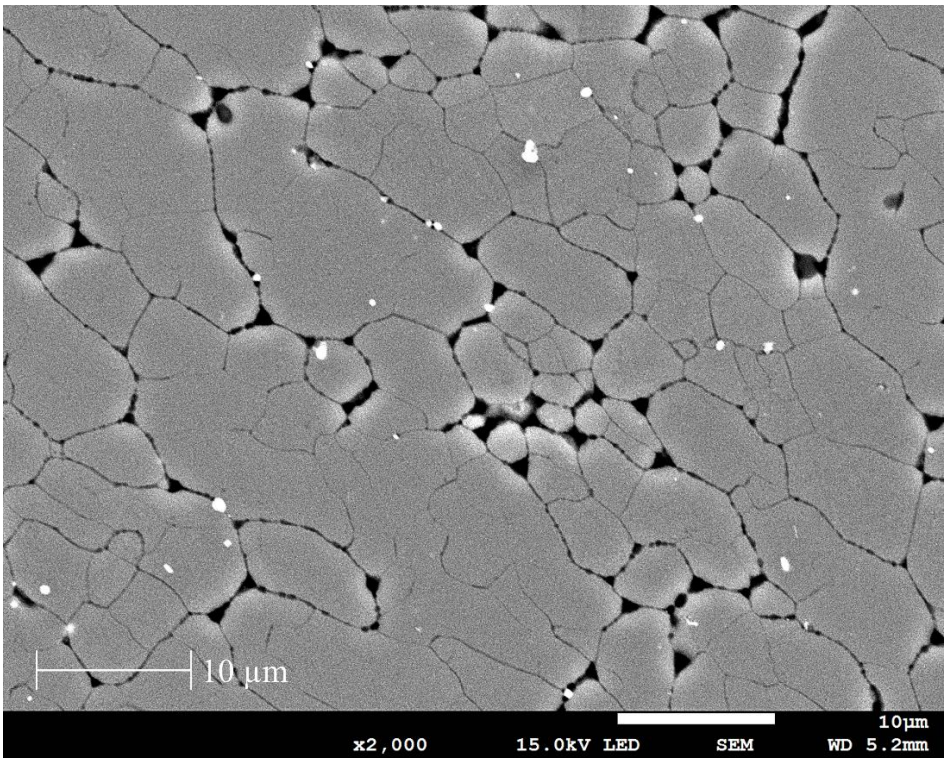

Figure 13.1: Microstructure of as-polished Alumec 89 aluminum surface used during frictional sliding tests.

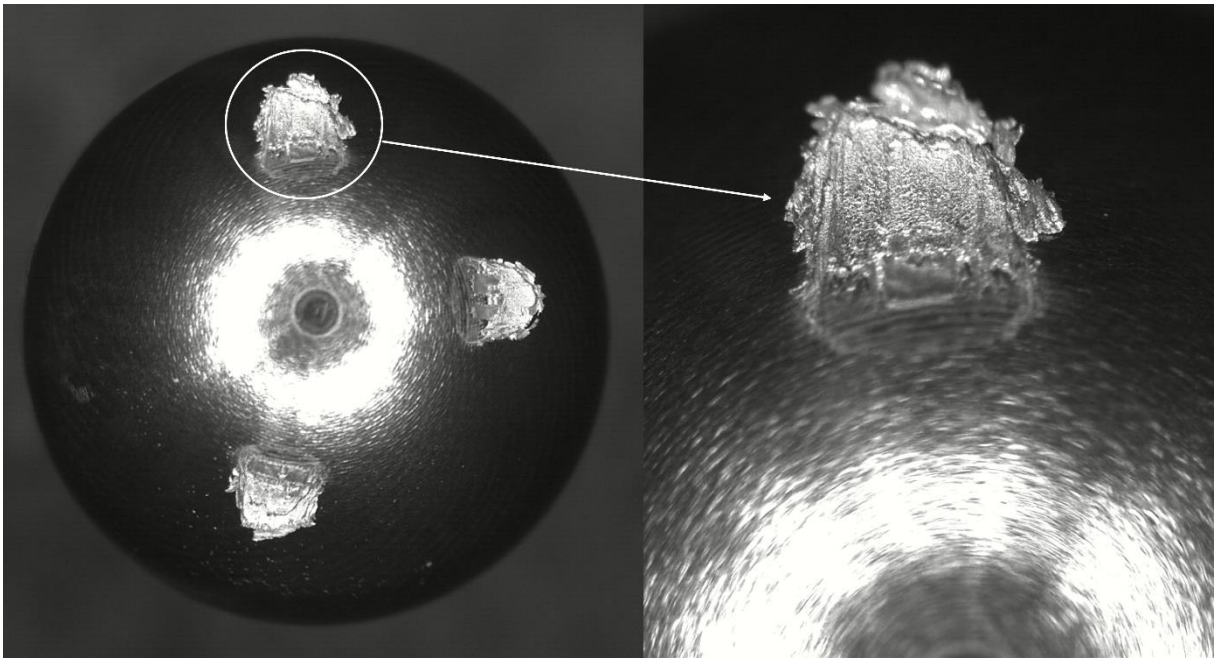

Figure 13.2: LOM image exemplifying the location of contact interaction between pin and workpiece surfaces during pin-turning tests.

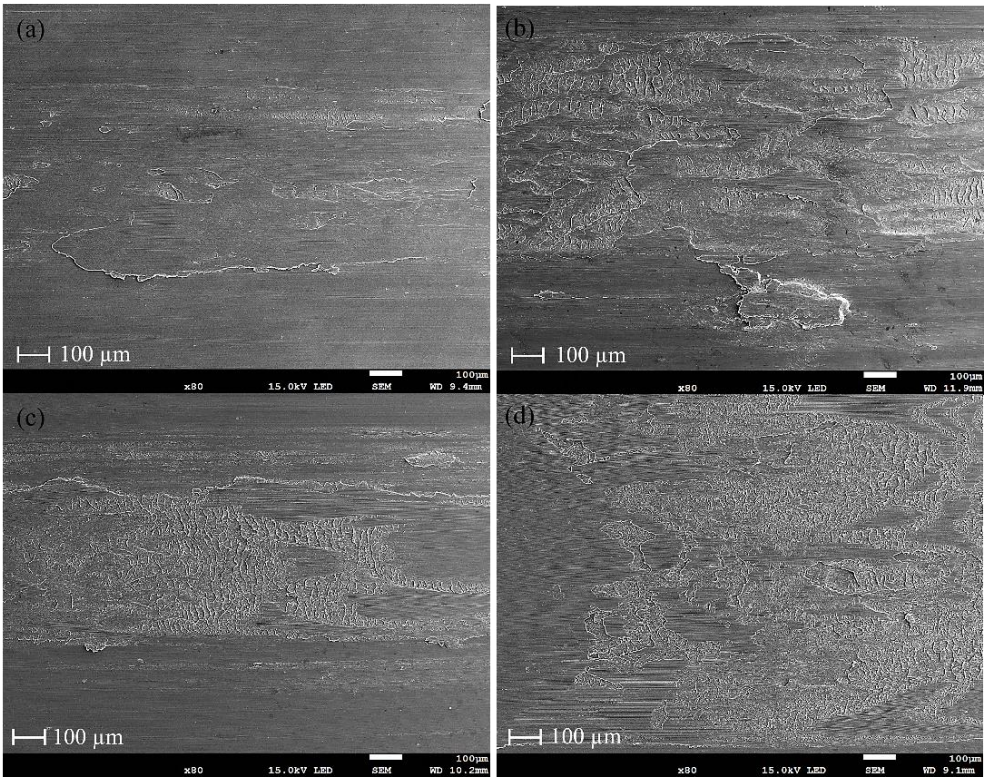

Figure 13.3: Sliding tracks generated during pin-turning tests of WC-Co pins against Alumec 89 workpiece. (a) Sliding track at 5s - 600 m/min test. (b) Sliding track at 30 s - 600 m/min test. (c) Sliding track at 5 s - 1200 m/min test. (d) Sliding track at 30 s – 1200 m/min test.

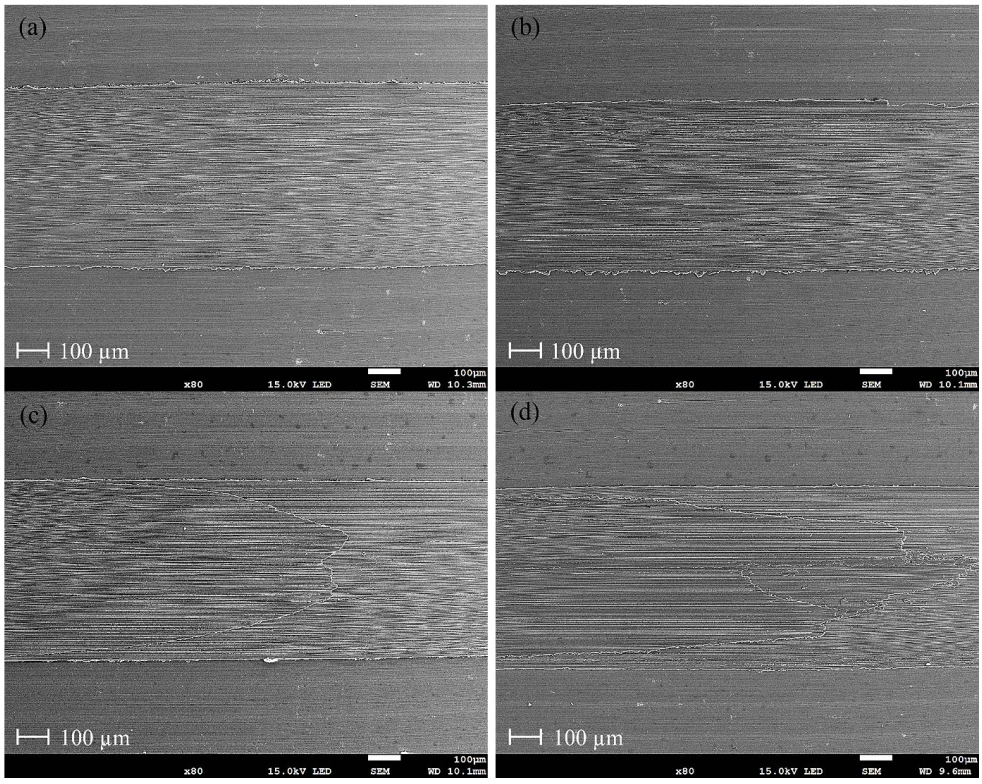

Figure 13.4: Sliding tracks generated during pin-turning tests of CVD coated pins against Alumec 89 workpiece. (a) Sliding track at 5s - 600 m/min test. (b) Sliding track at 30 s - 600 m/min test. (c) Sliding track at 5 s - 1200 m/min test. (d) Sliding track at 30 s – 1200 m/min test.

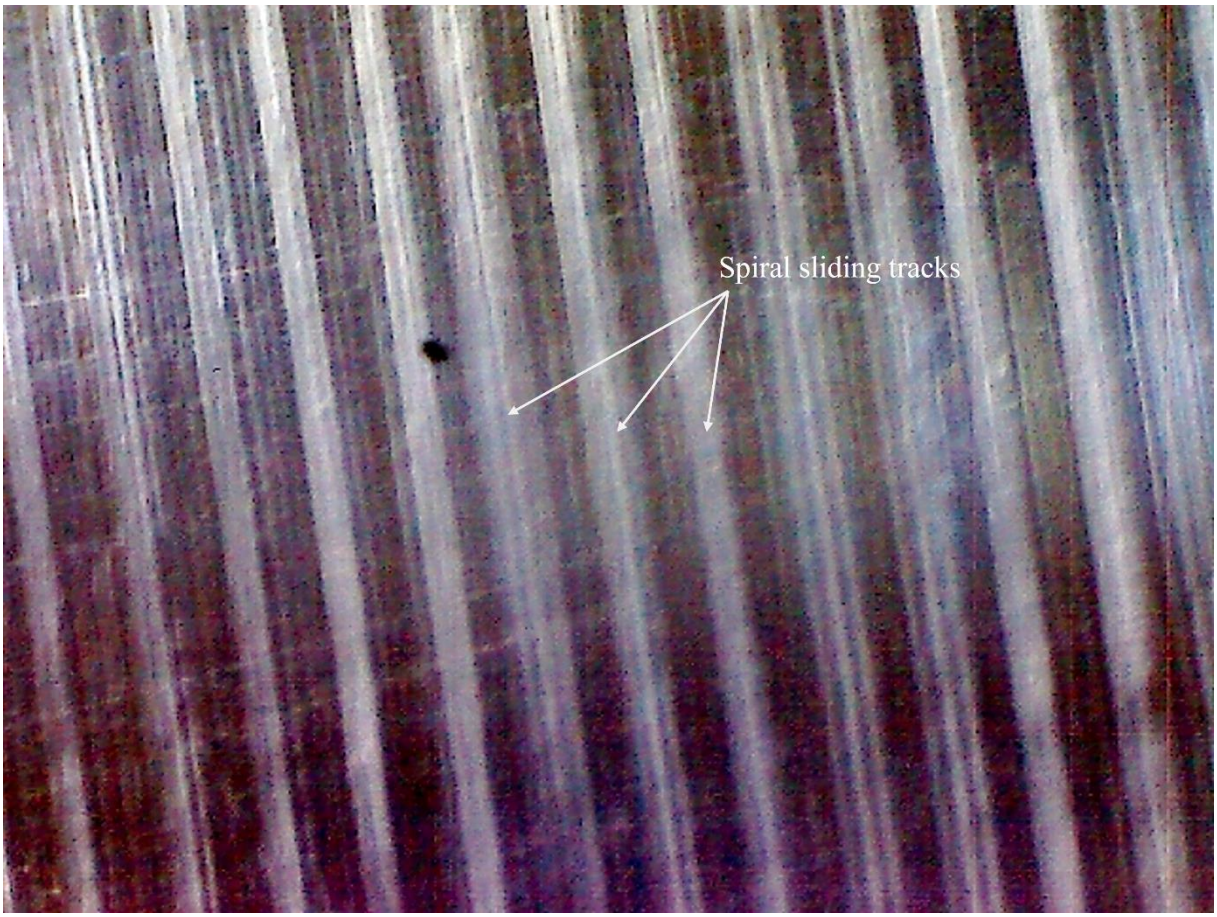

Figure 13.5: Spiral sliding tracks generated by WC-Co cemented carbide pin on Alumec 89 workpiece surface during open pin-turning.

.

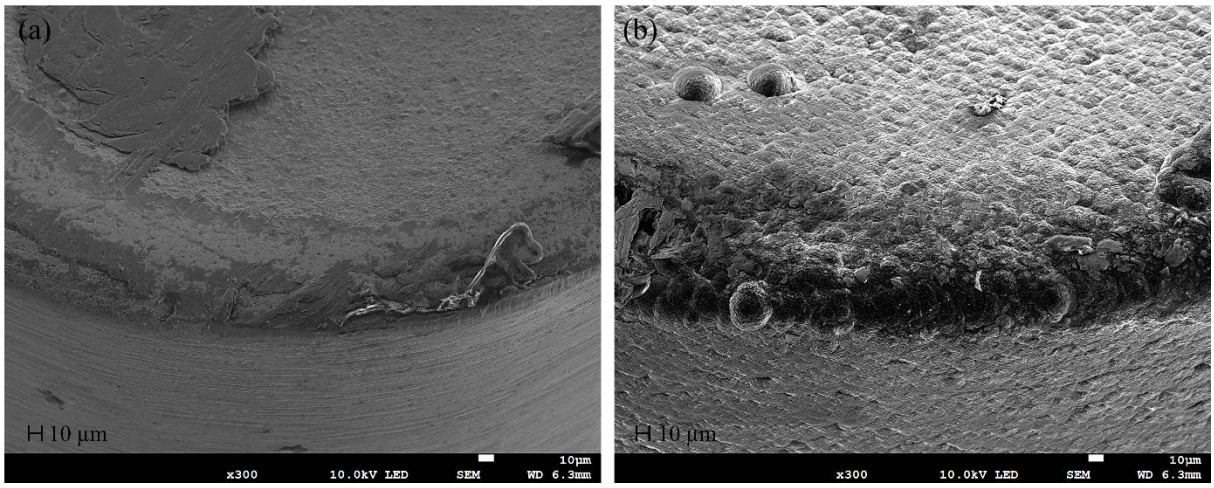

Figure 13.6: Enhanced SEM images of material transfer characteristics at the cutting edges of (a) WC-Co cemented carbide and (b) CVD coated cutting tools. Both images taken from test preformed under 5 s continuous workpiece interaction at a cutting speed of 600 m/min.

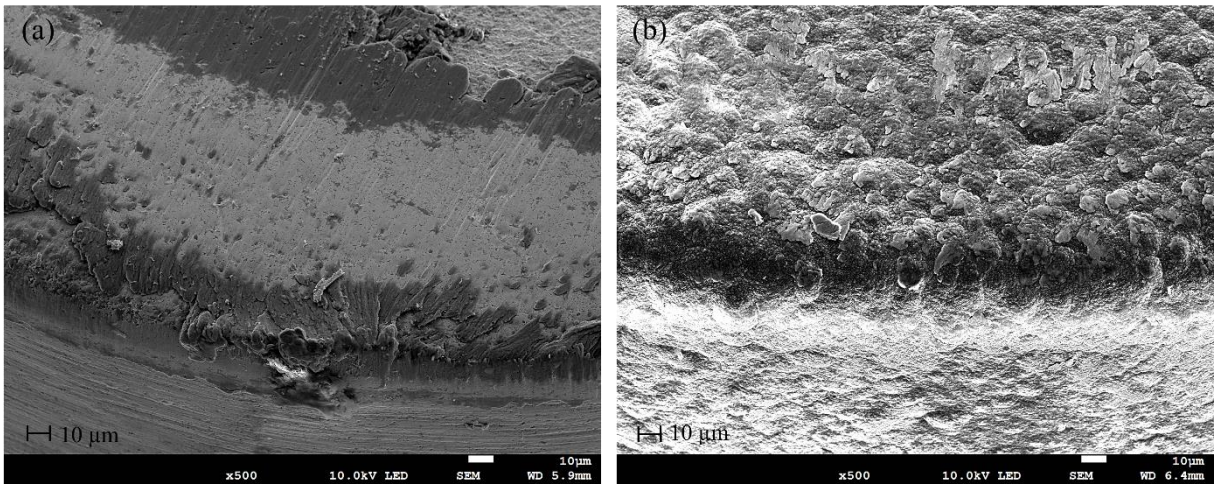

Figure 13.7: Enhanced SEM images of material transfer characteristics at the cutting edges of (a) WC-Co cemented carbide and (b) CVD coated cutting tools. Both images taken from test preformed under 60 s continuous workpiece interaction at a cutting speed of 600 m/min.

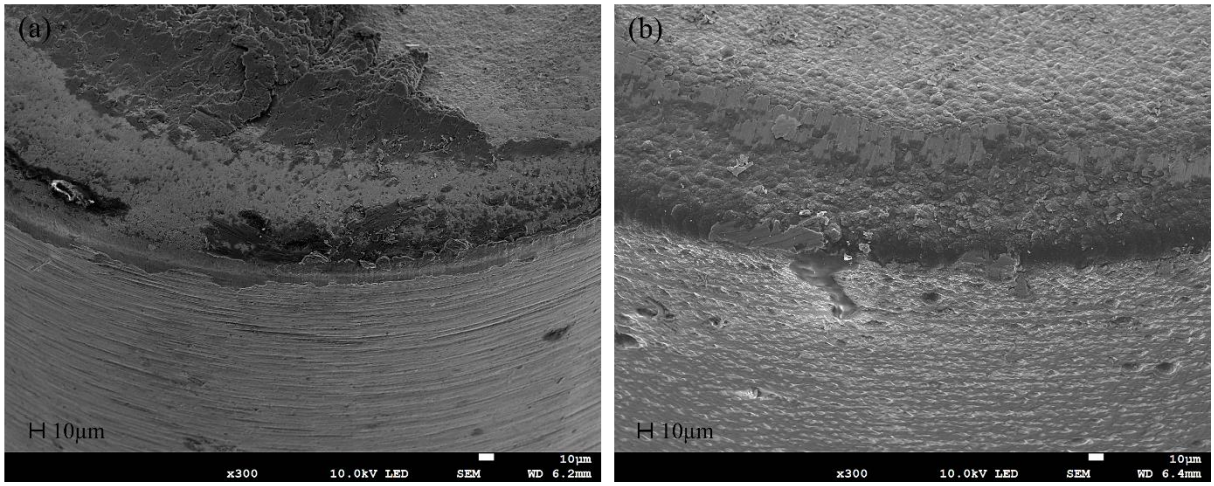

Figure 13.8: Enhanced SEM images of material transfer characteristics at the cutting edges of (a) WC-Co cemented carbide and (b) CVD coated cutting tools. Both images taken from test preformed under 5 s continuous workpiece interaction at a cutting speed of 1200 m/min.

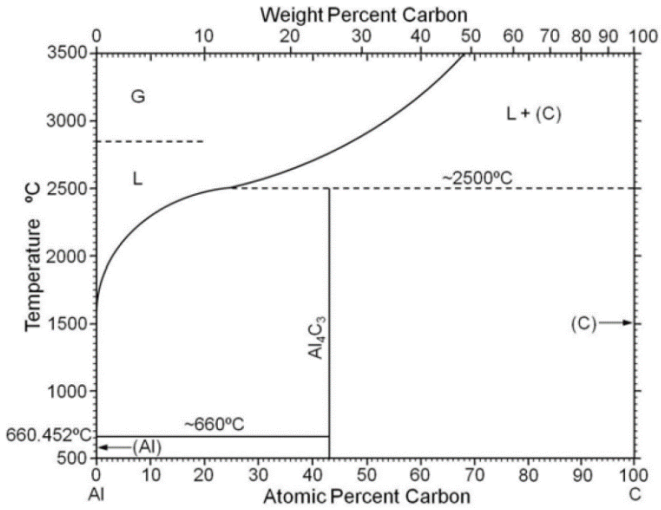

Figure 13.9: Phase diagram of C-Al system in the temperature range of 500-3500 °C [29].

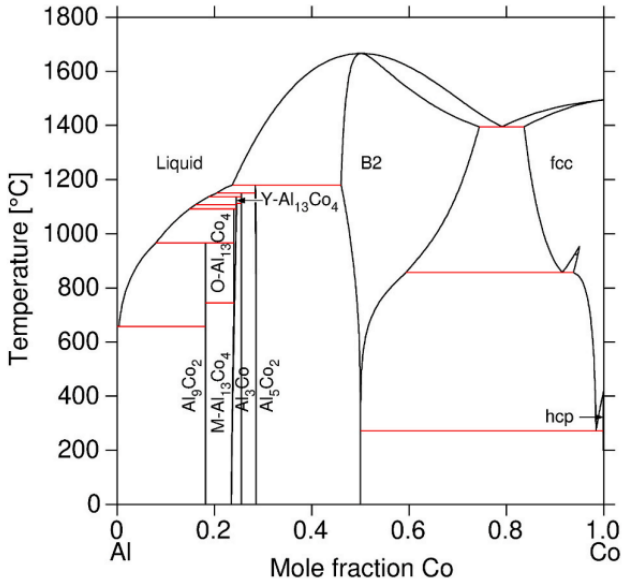

Figure 13.10: Phase diagram of Co-Al system in the temperature range of 0-1800 °C [30].